



Iron oxidation in groundwater

using a hyperbolic water vortex system



Graduation internship

Esther de Kroon

Iron oxidation in groundwater using a Hyperbolic water vortex system

*Graduation internship Environmental Sciences & Chemical Engineering
November 2020 – April 2021*

Author

Esther de Kroon

esther.dekroon@hvhl.nl

Student nr. 000012200

Company

Wetsus European Centre of Excellence for sustainable water technology
Oostergoweg 9, 8911 MA Leeuwarden

Supervisors Wetsus

dr. ir. Luewton Lemos F. Agostinho

Professor (Lector) Water Technology, NHL Stenden University of Applied Sciences

luewton.agostinho@hvhl.nl

luewton.agostinho@nhlstenden.nl

Maarten van de Griend

Wetsus PhD Candidate

Maarten.vandeGriend@wetsus.nl

Supervisors VHL

Sandra Bruinenberg

Environmental Sciences

sandra.bruinenberg@hvhl.nl

Petra van Dalfsen

Chemical Engineering

petra.vandalfsen@hvhl.nl

Education

Environmental Sciences & Chemical Engineering
Van Hall Larenstein University of Applied Sciences
Agora 1, 8934 CJ Leeuwarden

Location

Agora 1, 8934 CJ Leeuwarden

Date

09-06-2021



university of
applied sciences



van hall
larenstein
university of applied sciences

Preface

Before you is the thesis “Iron oxidation in groundwater using a Hyperbolic water vortex system”, conducted in the context of the graduation for the studies Environmental Sciences and Chemical Technology at Van Hall Larenstein (VHL) and NHL Stenden Universities of Applied Sciences. The project was commissioned by Wetsus, European Centre of Excellence for Sustainable Water Technology and conducted in cooperation with NHL Stenden Lectorate Water Technology.

The lectorate combines business activities, education and research in order to solve issues regarding physical water- processes and technologies (NHL Stenden, 2020). This is achieved by cooperating with several partners such as Wetsus, a not-for-profit foundation located in Leeuwarden, the Netherlands, that facilitates multidisciplinary collaboration between companies and research institutes on the field of sustainable water technology. This results in a unique innovation model that contributes to the solution of the global water problems. Both the industry and the research institutes implement research within the (inter)national scientific programs in Wetsus. This research is then carried out by PhD-students and their supervisors as a four-year long research project at the Wetsus Laboratory (Wetsus, 2020a).

One such research project is ‘Vortex treatment of water in a hyperbolic geometry’ by Maarten van de Griend, a PhD-candidate at Wetsus and the BOKU University of Vienna (Wetsus, 2020b). With the supervision of dr. ir. Luewton Lemos F. Agostinho, he studies two types of vortex systems as alternative aeration techniques for water treatment (Van de Griend MSc., et al., 2019). The graduation project described in this thesis is part of this PhD-research.

During this project I have had the chance to work on a challenging, yet inspiring and relevant subject regarding sustainability, that sparked my curiosity towards water technology further. I have much enjoyed the team efforts that is involved in projects from Wetsus and the lectorate, as well as the opportunities of joining interesting discussions and gaining new experiences and skills. I have found this to be a very inspiring learning environment.

For this I would like to thank Luewton Lemos F. Agostinho, Maarten van de Griend and Elmar Fuchs for their supervision from Wetsus and the lectorate Water Technology, as well as Sandra Bruinenberg and Petra van Dalfsen for their supervision from VHL and NHL Stenden. I would also like to thank Jan Tuinstra from Wetsus, who helped me many times (and very patiently) with the technical aspects of the experimental setups used in the project, and MBO-Life Sciences student Junior de Vries, who was of great help to me during some of the experiments. Lastly I would like to thank my parents, who have always supported me during my studies, though the good and the hard times, and have encouraged me to continue my study ambitions to the next step of pursuing a Master degree.

I hope you will enjoy reading this thesis.

Esther de Kroon

9th of June 2021, Leeuwarden

Summary

Around 60% of drinking water in the Netherlands is from groundwater, often containing high concentrations of dissolved iron. This is generally removed by aeration, which is an important process in both drinking- and waste water treatment. The known disadvantages are high energy consumption relative to the aeration capacity and being prone to clogging. This makes aeration an expensive part of water treatment processes, accounting for 45-75% of total operational costs. This ensures that new, innovative aeration methods that are more sustainable and energy efficient are always in demand.

One such innovative aeration method is the hyperbolic funnel, invented by Walter Schauburger and based on the principles of Viktor Schauburger. Walter Schauburger applied the natural phenomena of vortices for improving water quality. The hyperbolic funnel consists of a cylindrical top part and an hyperbolically shaped bottom part. The vortex formed in the funnel provides the formation of a large air-water interface compared to the liquid volume present in the system, resulting in the expectation of being a suitable system for aeration. Three different flow regimes have been identified from previous experiments, each with characteristic interfaces and aeration capacities; the Restricted Schauburger (RS), the Twisted Schauburger (TS) and the Straight Schauburger (SS). However, the actual performance in terms of aeration- and iron oxidation efficiency of the hyperbolic funnel and the possibilities for upscaling was still unknown. The evaluation of these aspects was the main objective of this research.

The first part of the research consisted of the generalization of the system, during which the flow rate and backpressure were monitored, as well as Dissolved Oxygen (DO), pH and Oxidation-Reduction Potential (ORP) at the inlet and outlet of the system. Tracer experiments were performed to verify Hydraulic Retention Time (HRT), liquid volume and flow behaviour of each flow regime. Fe^{2+} and Fe^{3+} concentrations were measured at the inlet and outlet of the system for each flow regime and under various pH conditions to determine the iron oxidation efficiency. Lastly, the possibilities for upscaling were explored by recreating the flow regimes in a larger version of the hyperbolic funnel and comparing both systems.

The experiments have shown that the different flow regimes can be characterized based on three parameters: flow rate, pressure and DO. The acquired DO increase is reached within a very short HRT of 14-37 seconds. The tracer experiments show that the system behaves like a plug-flow reactor with longitudinal mixing. Of the three regimes, the TS possesses the largest aeration and iron oxidation capacity and can reach higher aeration efficiencies compared to other systems. In first instance the hyperbolic funnel seems to perform less compared to other aeration systems in terms of iron oxidation. However, unlike the other system, the efficiencies achieved by the funnel are reached within very short HRT. By increasing the pH and contact time after aeration, the TS is capable of reaching similar to higher oxidation efficiencies compared to other aeration methods. Upscaling showed little coherence in defining parameters between the two systems, due to differences in geometry and material of the funnels. Further research is required to determine and validate a suitable non-dimensional number that can facilitate upscaling.

Based on the research results, it is recommended to perform further experiments on optimization of the funnels operation and its application in iron oxidation. This includes tracer experiments from the gas phase, precise determination of the interface area, the effect of increased oxygen content in the gas phase for enhanced gas transfer, determining the aeration and iron oxidation efficiencies of the upscaled system and comparing a variety of systems (size and materials) for composing a non-dimensional number. For optimizing the iron oxidation, it is recommended to evaluate the effect of prolonging aeration and/or contact time after aeration and selection of pH-dosing chemicals, so that lower pH conditions might be applied for the iron oxidation process while minimizing chemical usage.

Samenvatting

Ongeveer 60% van het drinkwater in Nederland is afkomstig van grondwater, wat vaak opgelost ijzer bevat. Dit wordt veelal verwijderd door middel van beluchting, een belangrijk proces voor de behandeling van zowel drinkwater als afvalwater. Bekende nadelen bestaan uit hoog energie verbruik ten opzichte van beluchtingscapaciteit en gevoeligheid voor verstopping. Dit maakt beluchting een duur onderdeel van (afval)waterbehandeling, verantwoordelijk voor 45-75% van totale operationele kosten. Hierdoor is er altijd vraag naar nieuwe innovatieve en duurzame beluchtingsmethoden.

Een voorbeeld van zo'n innovatieve methode is de hyperbolische trechter, ontwikkelt door Walter Schauburger en gebaseerd op de principes van Viktor Schauburger. Walter Schauburger paste het natuurlijke fenomeen van vortices toe voor verbetering van waterkwaliteit. De hyperbolische trechter bestaat uit een cilindervormige bovenkant en een hyperbolische onderkant. De gevormde vortex bevat een groot lucht-water interface ten opzichte van het water volume in het systeem, resulterend in de verwachting dat het een geschikte beluchtingsmethode is. Drie verschillende stromingsregimes zijn in voorgaande experimenten bepaald; de Restricted Schauburger (RS), de Twisted Schauburger (TS) en de Straight Schauburger (SS). Echter, de prestatie wat betreft beluchtungs- en ijzer oxidatie efficiëntie van de trechter en het effect van opschaling waren nog grotendeels onbekend. De doelstelling van dit onderzoek bestond uit de evaluatie van deze aspecten.

Het eerste deel van het onderzoek bestond uit de generalisatie van het systeem, waarbij werd gemonitord op debiet en druk, als ook op opgelost zuurstof (DO), pH en Oxidatie Reductie Potentiaal (ORP) bij de in- en uitlaat. Tracer experimenten zijn uitgevoerd voor het verifiëren van de verblijfstijd (HRT), watervolume en stromingsgedrag van elk regime. Fe^{2+} en Fe^{3+} concentraties bij de in- en uitlaat zijn gemeten voor elk regime en onder verschillende pH condities voor de bepaling van de ijzer oxidatie efficiëntie. Ten slotte zijn de mogelijkheden voor opschaling verkend door het reproduceren van de regimes in een grotere versie van de hyperbolische trechter ter vergelijking van beide systemen.

Uit de experimenten blijkt dat de verschillende regimes gekarakteriseerd kunnen worden op basis van drie parameters; debiet, druk en DO. De verkregen DO wordt bereikt binnen een zeer korte HRT van 14-36 seconden. De tracer experimenten tonen aan dat er een plug-flow stroming met longitudinale mixing in de trechter aanwezig is. Van de drie regimes bevat de TS de grootste beluchtungs- en ijzer oxidatie capaciteit en bereikt een hogere beluchtungs-efficiëntie dan andere beluchtungs-methoden. In eerste instantie lijkt de hyperbolische trechter minder goed te presteren dan andere beluchtungs-methoden wat betreft ijzer oxidatie. Echter, in tegenstelling tot andere systemen worden de efficiënties van de hyperbolische trechter bereikt binnen een zeer korte HRT. Door toepassing van hogere pH en reactietijd na beluchting is de TS in staat om vergelijkbare tot hogere oxidatie efficiënties te bereiken dan andere beluchtungs-methoden. Opschaling liet weinig samenhang zien tussen beide trechters door verschillen in geometrie en materialen. Vervolgonderzoek is nodig voor verdere bepaling en validatie van een geschikt non-dimensionaal nummer.

Gebaseerd op de onderzoeksresultaten wordt aanbevolen tot vervolgonderzoek gericht op optimalisatie van de werking van de trechter en de toepassing in ijzer oxidatie. Dit omvat tracer experimenten vanuit de gas fase, nauwkeurige bepaling van het interface oppervlakte, het effect van verhoogde zuurstof concentratie in de gas fase, bepaling van beluchtungs- en ijzer oxidatie efficiënties van de grotere trechter en vergelijking van meerdere systemen (afmeting en materialen) voor het opstellen van een non-dimensionaal nummer. Voor de optimalisatie van ijzer oxidatie wordt aanbevolen om het effect van verlenging van beluchtungs- en/of contact tijd na beluchting te beoordelen en de selectie van pH-doseringsschemaliën, zodat lagere pH condities toegepast kunnen worden voor het ijzer oxidatie proces en chemicaliën gebruik geminimaliseerd kan worden.

Table of Content

1. Introduction.....	1
1.1 Background.....	1
1.2 Problem definition.....	1
1.3 Main objective.....	1
1.4 The hyperbolic vortex and sustainability.....	2
1.5 Readers guide.....	3
2. Theoretical background.....	4
2.1 Vortex technology and principles.....	4
2.2 Aeration and gas transfer.....	5
2.3 Aeration efficiency.....	8
2.4 Iron oxidation.....	9
3. Methodology.....	11
3.1 Generalization.....	11
3.2 Iron oxidation.....	12
3.3 Upscaling.....	13
4. Results.....	14
4.1 Generalization results.....	14
4.2 Iron oxidation results.....	19
4.3 Upscaling results.....	21
5. Discussion.....	24
6. Conclusion.....	26
7. Recommendations.....	27
References.....	29
Appendix.....	32
Appendix I: Composition groundwater and tap water.....	I
Appendix II: Information Experimental setups F01 and F02.....	II
Appendix III: Vortex characteristics and photographs.....	IV
Appendix IV: Data generalization experiments.....	VI
Appendix V: Volume calculations hyperbolic funnel and vortices.....	VIII
Appendix VI: Graphs and calculations tracer experiments.....	XI
Appendix VII: Results water sample analysis iron oxidation efficiency.....	XIV

Nomenclature and acronyms

Abbreviation	Description	Units
A	Area	cm ²
C	Concentration	mg/L or mol/L
C_g	Concentration of species in gas phase	mg/L or mol/L
C_L	Concentration of species in liquid phase	mg/L or mol/L
C_L[*]	Concentration of species in liquid phase at saturation	mg/L or mol/L
DO	Dissolved Oxygen	mg/L
D/uL	Dispersion number	
Eh	Electrical potential	mV or V
F	Faraday constant = 23061	cal/V
H	Henry's constant	
HRT	Hydraulic Retention Time	s
K	Equilibria constant	
K_La	Volumetric mass transfer coefficient	h ⁻¹
K_La₂₀	Volumetric mass transfer coefficient at 20 °C	h ⁻¹
ORP	Oxidation-Reduction Potential	mV or V
p	Pressure	millibar
P	Power	kW
Q	Flow rate	L/min or m ³ /h
r	Transfer rate	(mg/L)/min or (mg/L)/h
R	Gas constant = 1.987	cal/degree
RS	Restricted Schauburger	
RSF	Rapid Sand Filtration	
RTD	Mean Residence time Distribution	s
SAE	Standard Aeration Efficiency	kg O ₂ /kWh
SOTR	Standard Oxygen Transfer Rate	kg O ₂ /h
SS	Straight Schauburger	
\bar{t}	Mean residence time	s
TRL	Technical Readiness Level	
TS	Twisted Schauburger	
τ	Hydraulic Retention Time	s
V	Volume	L or m ³
WAC	Water Application Centre	

1. Introduction

1.1 Background

Aeration is a frequently used technique in drinking- and wastewater treatment processes for improving water quality and removing soluble ions and organic matter. The most common methods applied in water treatment are mechanical- and diffused aeration (Gray, 2010). However, both methods have disadvantages such as clogging and high energy requirements, contributing 45-75% of the total energy usage of (waste) water treatment (Rosso, Stenstrom, & Larson, 2008). These characteristics of aeration ensure that new, more efficient and sustainable aeration methods are always in demand.

One such method is inspired by Austrian forester and pioneer in biomimetics Viktor Schaubberger, who looked at nature for solving modern technical problems. Based on these principles his son Walter Schaubberger invented an water treatment technique that uses a water vortex. The hyperbolic vortex studied in the research of Maarten van de Griend is inspired by the principles of Schaubberger. It would be a more sustainable aeration method that does not possess the disadvantages of the conventional methods (Van de Griend MSc., et al., 2019). The vortex that is formed in the hyperbolic funnel creates an air-water interface due to the spiraling motion, and the air-suction created in its core causes more air to enter in order to equalize the pressure inside the system to the external pressure (Hill, 2017), therefore facilitating aeration.

A possible application for the Hyperbolic vortex is the oxidation of iron in groundwater, as part of drinking water treatment. By applying aeration, iron oxidation occurs after which the iron precipitates and can be separated by filtration. Further explanation of the subjects discussed in this paragraph can be found in **CHAPTER 2. THEORETICAL BACKGROUND.**

1.2 Problem definition

The performance of the Hyperbolic vortex in terms of aeration- and iron oxidation efficiency is currently unknown. The system still has a low Technology Readiness Level (TRL) of around 4-5, meaning that it is tested only on laboratory scale, thus knowledge of its functioning and performance under real scale conditions is still lacking (Innovencio, 2017). Within the Applied Water Physics Theme of Wetsus, there are companies interested in the suitability of the system as an aeration method and its applications, such as iron oxidation in groundwater. Extensive testing of the system was therefore required in order to determine its performance and exploring upscaling possibilities. During these tests, the aeration- and iron oxidation efficiency was to be determined under various conditions and the influence of flow regimes and pH conditions were to be evaluated for optimized performance.

1.3 Main objective

The main objectives of this project were to investigate the aeration- and iron oxidation efficiency under various flow regimes and pH conditions and the generalization of the Hyperbolic vortex so that upscaling towards a TRL of 6-7 could be explored. For this, it was evaluated if a non-dimensional number could be proposed to generalize the system and facilitate upscaling. The volumetric mass transfer coefficient K_{La} for oxygen was calculated, which gives an indication of the capability of a system for oxygen transfer. The parameters dissolved oxygen (DO), oxidation-reduction potential (ORP), pH and iron concentrations were measured at the in- and outlet. Based on these parameters, the aeration- and iron oxidation efficiency was determined and the system was evaluated for its suitability as an aeration method for iron oxidation in groundwater.

1.3.1 Research questions

The following research question was formulated in order to reach the objective of the project:

- Is the Hyperbolic vortex suitable as an alternative aeration method for iron oxidation in groundwater?

Several sub questions were formulated to assist in answering the main research question:

Generalization

1. What are the main parameters which can be used to characterize the flow regimes within the system?
2. What are the volumetric mass transfer coefficient ($K_L a$) values of oxygen and aeration efficiencies of the flow regimes and their transition phases?
3. How does the system compare to other aeration methods currently in use in terms of efficiency and sustainability?

Iron removal

4. What are the iron oxidation efficiencies of the system under various flow regimes and pH conditions?
5. Which criteria should be met in terms of iron removal from groundwater?
6. How does the system compare to other aeration methods currently in use in terms of iron oxidation?

Upscaling

7. Can non-dimensional numbers be applied for generalizing the system to facilitate upscaling? And if yes, which are they?

1.4 The hyperbolic vortex and sustainability

As mentioned previously, aeration is an energy intensive process accounting for a large portion of water treatment costs. Lowering this energy demand therefore contributes substantially to increased sustainability of water treatment. For instance, many waterboards are working towards being energy neutral in 2025, decreasing their climate-footprint as much as possible as their responsibility towards society (Unie van Waterschappen, 2018).

The hyperbolic vortex was inspired by many natural phenomena occurring as vortices such as whirlpools, whirlwinds and hurricanes (Tsuji & Müller, 2019). The occurrence of vortices in nature suggests that this is a favourable shape in terms of efficiency, since nature often finds the most efficient way by evolution and the fundamental laws of physics. For this reason, many technologies have already been inspired, designed and optimized by applying Biomimetics (Bhushan, 2009). The use of potential energy in the formation of the vortex, combined with the naturally occurring air-suction towards the core and a favourable ratio between the air-water interface area and the water volume, raises the expectation that the hyperbolic vortex is more energy efficient than other aeration systems. Combining this with the reduction of clogging problems that many other aeration systems encounter (therefore requiring more maintenance and (chemical) cleaning), describes the systems possible contribution towards sustainability.

Besides reduction in chemical usage due to clogging problems, the chemical usage for the iron oxidation process is also an important consideration. Iron oxidation depends on pH, therefore chemicals are often dosed for increasing the pH to more favourable conditions. By applying the lowest possible pH for iron oxidation, chemical usage can be minimized. The type of chemical also influences the sustainability of the process, for instance by selecting green chemicals. These type of chemicals are

considered less harmful to the environment throughout its life-cycle and are designed to reduce or eliminate the use of more hazardous chemicals (Anastas & Warner, 1998) (Anastas & Zimmerman, 2003). Optimizing chemical usage and selection contributes further to the sustainability of iron removal in groundwater.

1.5 Readers guide

The first chapter of this report shows a short introduction of the project and its objectives, while the theoretical background in chapter two provides a more in-depth look for the reader about relevant subjects. The methods used for this project are described in chapter three, after which the results are presented and discussed in chapter four. Chapter five contains the discussion of proceedings and circumstances that could have had an influence on the research results. Finally, the outcome of the research is summarized in chapter six as the conclusion, followed by the corresponding recommendations in chapter seven.

2. Theoretical background

In 2019, the Dutch drinking water companies produced about 1.2 billion m³ of (tap) water (Drinkwater Platform, 2020). Just over 60% of this is derived from groundwater sources and primarily used in households (CLO, 2020). Groundwater consists mainly of rainwater that has percolated into the soil and gathers in layers of porous rocky material saturated with water, called aquifers (NGWA, 1999). Groundwater often contains dissolved iron, which is removed during treatment for drinking water. The official limit of iron in drinking water in the Netherlands is set at 0.2 mg/L (Rijksoverheid, 2010).

2.1 Vortex technology and principles

The original founder for the application of vortex flows as water purification techniques is the Austrian Walter Schauburger (1914-1994), son of Viktor Schauburger (1885-1958, **Figure 1**). Viktor started his career as a forester, but later became a self-taught inventor. By observing nature, especially the behaviour of water and its interactions with the environment, he developed his theories and inventions. After all, nature often finds the most efficient way.



Figure 1: Viktor and Walter Schauburger, 1958

The vortex is one of such phenomena that is widespread in nature. By studying vortex flows in water and other natural phenomena, he developed his implosion theory. He applied this theory as a method for improving water quality (Coats, 1997). Due to his lack of formal education, controversial ideas and unusual methods, his theories were not widely accepted by the scientific community. After the death of Viktor Schauburger, his son Walter Schauburger (1914-1994) continued his work by formulating the mathematics for his father's theories and applying them by, for example, the invention of the hyperbolic funnel as water treatment device. (Radlberger, 2014) (Stichting Natuur- en Implosietechnieken, 2015).

2.1.1 Hyperbolic funnel

Schauburgers research resulted, among other things, in the development of the hyperbolic funnel as it is applied in this project. The funnel consists of a cylindrical part at the top and a hyperbolically shaped part at the bottom (see **Appendix II**). The tangential angle and horizontal position of the inlet located at the top of the funnel causes a spiraling flow by which the vortex arises. The inward and downward flow creates a sub pressure, pulling the surrounding air into the central air column.

In previous research of Wetsus performed by Nicolae Şişcanu (Şişcanu, 2020), three different flow regimes were established in the hyperbolic funnel, of which the dimensions can be found in **Appendix II**. By varying the flow rate and controlling the restriction at the outlet, various shapes of vortices were formed, each with a different air-water interface area and aeration properties (**Figure 2**). A short description of each regime is given in sequence;

- **TWISTED SCHAUBURGER (TS)**: established by applying a medium flow rate. The water level does not exceed 70-80mm, measured from the bottom of the cylinder up. The air column has a clear hyperbolic shape and shows a helical pattern. It has the largest surface area of the air-water interface of all flow regimes.
- **STRAIGHT SCHAUBURGER (RS)**: established by applying a higher flow, with the water level reaching the top lid of the cylinder. The column of the air-water interface changes to an almost cylindrical spiral that spans from top to bottom of the funnel. It has an intermediate surface area of the air-water interface compared to the other flow regimes.

- **RESTRICTED SCHAUBERGER (SS)**: by restricting the outlet, the backflow pressure is increased in the funnel. Combining this with a lower flow rate results in a conical air-water interface that only extends about 400-500mm downwards into the hyperbolic part. This regime has the lowest surface area of the air-water interface.

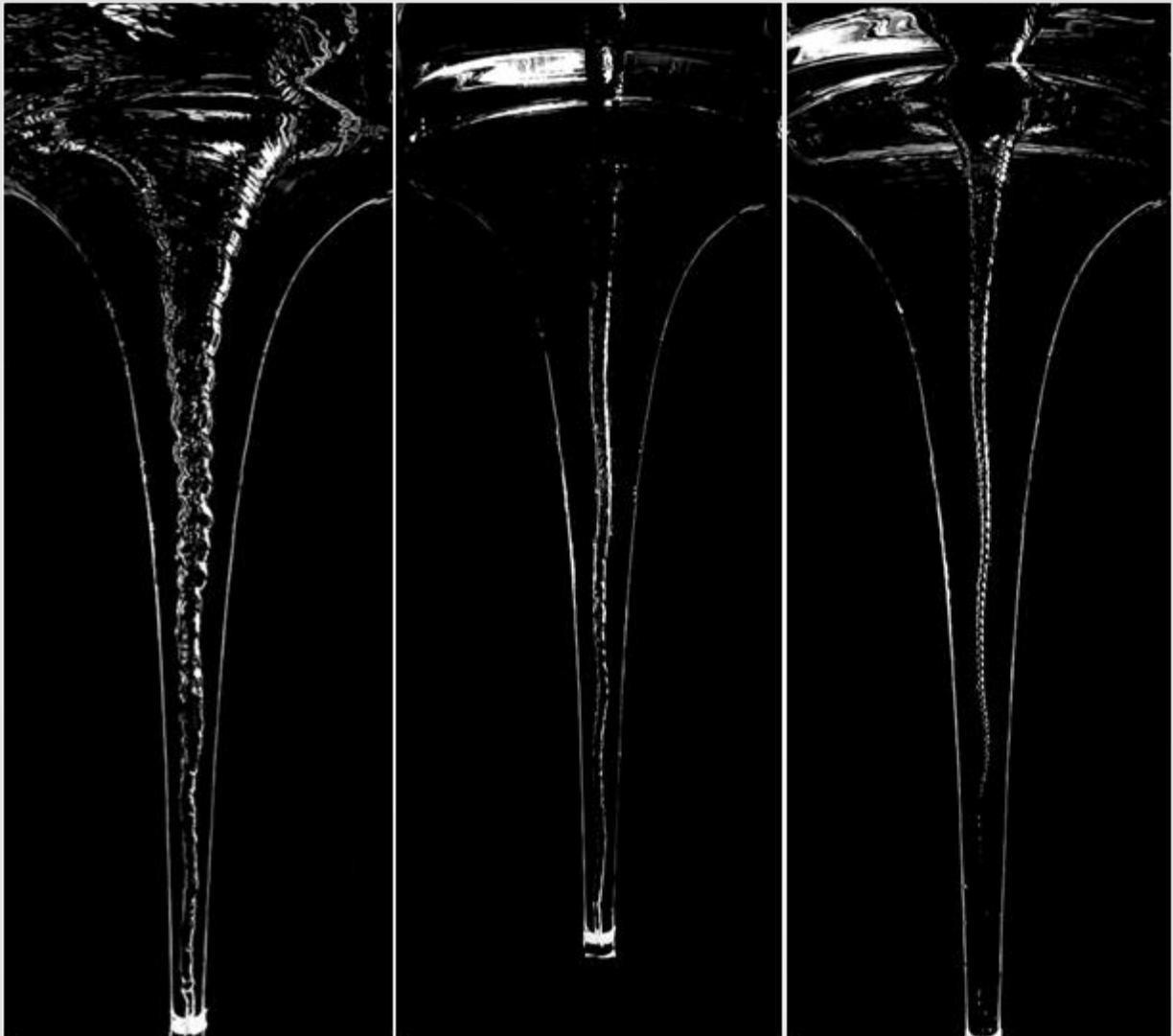


Figure 2 Contrast images of the three flow regimes within the hyperbolic funnel, f.l.t.r.: Twisted Schauberger (TS), Straight Schauberger (SS), Restricted Schauberger (RS). (Images by Nicolae Şişcanu, image editing by M. van de Griend)

2.2 Aeration and gas transfer

Aeration is a treatment step commonly applied for (ground)water, during which oxygen is added to water via diffusion from the air- and water phases. This leads to an increase in concentration of Dissolved Oxygen (DO) in the water. Aeration targets on increasing the air-water interface. Most common methods are mechanical aeration, diffusion aeration, cascades or tower aeration. Common disadvantages of mechanical- and diffused aeration primarily consist of the high power usage compared to the oxygenation capacity of the system (Gray, 2010). Besides this, diffused- and tower aeration are also sensitive for clogging and can be hindered by iron deposition (TU Delft, 2016).

The rate at which aeration takes place is primarily dependent on three factors; diffusion between the gas- and liquid phase (interface), mixing (advection) in the bulk gas and liquid, and biological or

chemical reactions within the system. The corresponding mass balance is as follows (Benjamin & Lawler, 2013);

$$\text{Rate of change of mass of } i \text{ stored in the control volume} = \text{Net change in mass of } i \text{ due to advection} + \text{Net change in mass of } i \text{ due to diffusion} + \text{Net change in mass of } i \text{ due to reactions}$$

Equation 1

Where i represents the species of gas that is transferred, in this case oxygen. This mass balance can also be written as an equation (Benjamin & Lawler, 2013);

$$V_L \frac{dC_L}{dt} = Q(C_{L,in} - C_L) + V_L \cdot K_L a (C_L^* - C_L) + V_L r_{biochem}$$

Equation 2

Where;

-	V_L	Liquid volume in reactor	(L)
-	Q	Flow rate	(L/h)
-	$K_L a$	Volumetric mass transfer coefficient	(h ⁻¹)
-	C_L	DO in bulk liquid	(mg/L)
-	$C_{L,in}$	DO in feed	(mg/L)
-	C_L^*	DO at saturation	(mg/L)
-	$r_{biochem}$	DO due to biochemical reactions	($\frac{mg/L}{h}$)

2.2.1 Diffusion

Transport of oxygen from the gas phase to the liquid phase is based on diffusion. This process is driven by a difference in concentration, so that an overall transfer of oxygen takes place between the two phases until an equilibrium is achieved (i.e. DO saturation). The relationship between the oxygen concentration in the liquid and gas phase at equilibrium is described by *Henry's law* (Benjamin & Lawler, 2013);

$$H = \frac{C_g}{C_L}$$

Equation 3

Where H is Henry's constant and C_g and C_L are the oxygen concentrations in the gas and liquid phase at equilibrium.

For the oxygen to pass from one phase to the other, the interface between the two phases must be crossed. This interfacial area consists of several regions (FIGURE 3); the bulk gas and liquid, the interfacial gas- and liquid layers, and the interface itself. This depiction of the interface is also known as the *two-film theory* of Walter G. Whitman (Whitman, 1923). The interfacial layers differ from the bulk material because the fluid dynamics in these regions are strongly influenced by the interface. They are the rate limiting step for gas transfer, because the motion of molecules is more restricted at the interface. This means that transport of molecules takes place by diffusion only, resulting in a

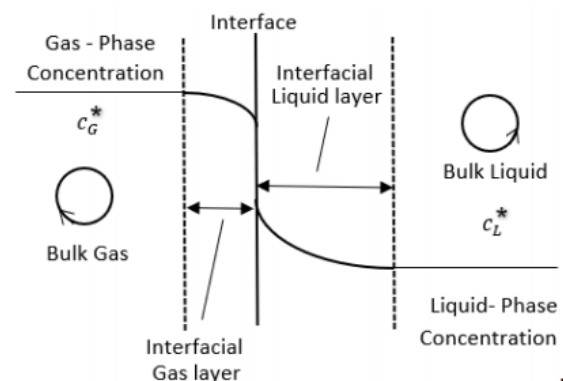


Figure 3 Schematic representation of the interfacial area (Benjamin & Lawler, 2013)

concentration gradient between the interface and the bulk material. Saturation near the interface can therefore limit the rate of oxygen transfer (Benjamin & Lawler, 2013).

2.2.2 Advection

According to the two-film theory, the interfacial layers consists of stagnant films; no transport of the liquid/gas in this region occurs due to advection, resulting into differences between theoretical predictions and experimental observations. This deviation was later corrected by the packet-exchange theory; the liquid is envisioned as a collection of small packets, which are brought from the bulk liquid to the interfacial layer, remain there for a certain amount of time during which diffusion takes place in the packet, and is taken up into the bulk liquid again as it is replaced by a new packet (Benjamin & Lawler, 2013). This exchange of packets requires advection in the bulk liquid, i.e. mixing. The thickness and the time spend by a packet in the interfacial layer is dependent on the mixing in the bulk liquid; enhanced mixing therefore improves gas transfer and reduces the effect of saturation near the interface.

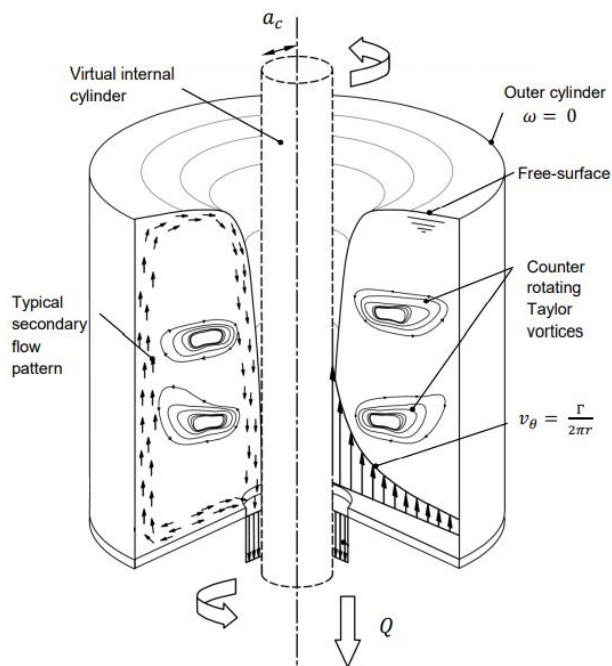


Figure 4 Simplified representation of the analogy between the vortex and the Taylor-Couette flow (Mulligan, 2015)

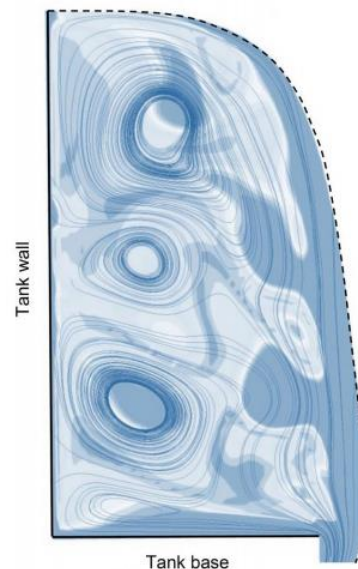


Figure 5 Model of the secondary flow pattern of a vortex (Mulligan, De Cesare, Casserly, & Sherlock, 2018)

When looking at a vortex such as in the hyperbolic funnel, the mixing is facilitated by a secondary flow pattern in the bulk liquid. This was studied by Sean Mulligan, who used a tank basin with a central draining point to induce a vortex. He proposed that the flow pattern of a vortex can be described as a Taylor-Couette flow; the movement of a liquid between two concentric cylinders that arises when one or both cylinders rotate (Mulligan, 2015). When translating this to the hyperbolic funnel, the outer wall can be seen as the (stationary) outer cylinder, while the air core acts as the rotating inner cylinder (FIGURE 4). When increasing the rotational speed of the inner cylinder, increasing turbulence is present in the bulk liquid, eventually resulting in the formation of smaller toroidal vortices stacked alongside the vortex (FIGURE 5). These are called Taylor vortices and provide the secondary flow pattern that enhances the internal mixing and gas transfer in the system (Mulligan, De Cesare, Casserly, & Sherlock, 2018).

2.3 Aeration efficiency

In order to evaluate and compare different aeration systems, it is necessary to determine the aeration efficiency. This efficiency is often expressed in several coefficients. Commonly used coefficients are the K_La , SOTR and the SAE.

2.3.1 Volumetric mass transfer coefficient (K_La)

The volumetric mass transfer coefficient (K_La) gives an indication of the capability of a system in facilitating oxygen transfer to the liquid phase. It is dependent on the liquid phase transfer coefficient (K_L) and the ratio between the liquid volume (V) and area of the interface (A), as shown in equation 4;

$$K_La = K_L \cdot \frac{A}{V}$$

Equation 4

The K_La can also be determined based on the oxygen mass balance (see equation 2), resulting in the following equation (Benjamin & Lawler, 2013);

$$K_La = \frac{Q}{V_L} \cdot \ln \left(\frac{C_L^* - C_{L,in}}{C_L^* - C_L} \right)$$

Equation 5

The K_La can be corrected to a standardized temperature of 20 °C, resulting in the K_La_{20} , by the following equation (Bunea & Ciocan, 2018);

$$K_La_{20} = K_La \cdot 1.024^{(20-T)}$$

Equation 6

Where T is the temperature in °C of the initial K_La value. Equation 5 was applied in this study for determining the K_La . The C_L was corrected for the oxygen consumption due to iron oxidation, of which the requirement of oxygen was based on stoichiometry (see paragraph **2.4.1 HOMOGENOUS OXIDATION**) and the mass balance for oxygen in the system;

$$C_{L,in} + C_{L,diff} = C_{L,out} + C_{L,Fe\ ox.}$$

Equation 7

Where $C_{L,in}$ is the initial DO of the inlet, $C_{L,diff}$ is the DO transferred to the liquid by diffusion, $C_{L,out}$ is the DO at the outlet and $C_{L,Fe\ ox.}$ the DO consumed by iron oxidation. Other biochemical reactions that could have an influence on the K_La were considered negligible based on the composition of the groundwater (APPENDIX I).

2.3.2 Standard Oxygen Transfer Rate (SOTR)

The SOTR gives the standard rate of oxygen that is transferred to the liquid phase by the system in kg O_2/h and is determined by the following equation;

$$SOTR = K_La_{20} \cdot C_L^* \cdot V$$

Equation 8

2.3.3 Standard Aeration Efficiency (SAE)

The SAE indicates how efficient the system is in terms of power consumption (P in kW) when transferring oxygen in kg O_2/kWh and is determined by the following equation;

$$SAE = \frac{SOTR}{P}$$

Equation 9

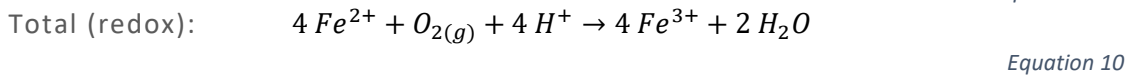
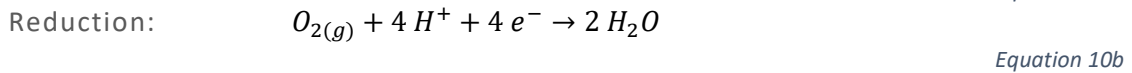
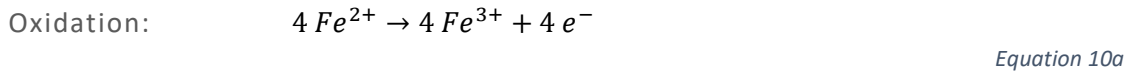
2.4 Iron oxidation

Oxygen is a strong oxidizer due to its high electronegativity. The addition of DO to groundwater triggers the oxidation of dissolved ferrous iron(II) (Fe^{2+}) to form the less soluble ferric iron(III) (Fe^{3+}), after which precipitation takes place and the iron can be removed by means of filtration (TU Delft, 2016).

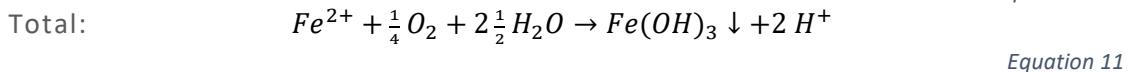
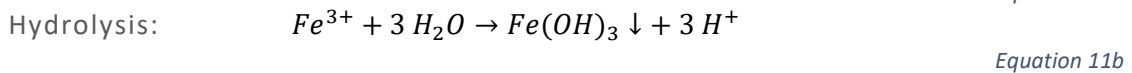
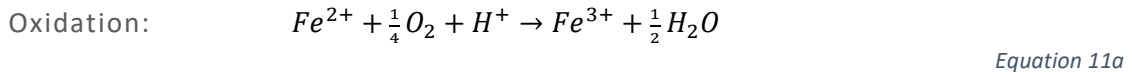
There are three different types of iron oxidation; homogeneous-, heterogeneous- and biological oxidation. All three types of oxidation generally take place during a typical iron removal process from groundwater. However, their contribution to iron removal depends on the circumstances of the process (van Beek, et al., 2016). This project focusses on homogeneous oxidation of iron.

2.4.1 Homogenous oxidation

Homogeneous iron oxidation is driven by the transfer of electrons through an oxidizing agent, in this case dissolved oxygen. The oxidation of ferrous iron and reduction of oxygen is given in equation 10 as half reactions, followed by the complete redox reaction.



The ferric iron(III) that forms reacts further with water molecules during a hydrolysis reaction. Iron(III)hydroxide ($Fe(OH)_3$) is formed as a result, which is insoluble in water and therefore precipitates out of solution. This reaction is shown in equation 11;



As can be seen in the equations above, the presence of oxygen (O_2) and a higher pH (OH^{-}) is required for homogeneous oxidation to take place.

2.4.2 pE-pH relation in iron oxidation

Like many other solute species in natural waters, the stability of iron species is highly dependent on both pE and pH. Similar to pH, pE is a logarithmic scale and represents the electron activity; low pE indicates reducing conditions and high pE indicates oxidizing conditions. The transfer of electrons during a redox reaction is often accompanied by transfer of H^{+} ions, which means there is a close relation between redox and acid-base processes in an aquatic system. This relation and its effect on the stability of solute species

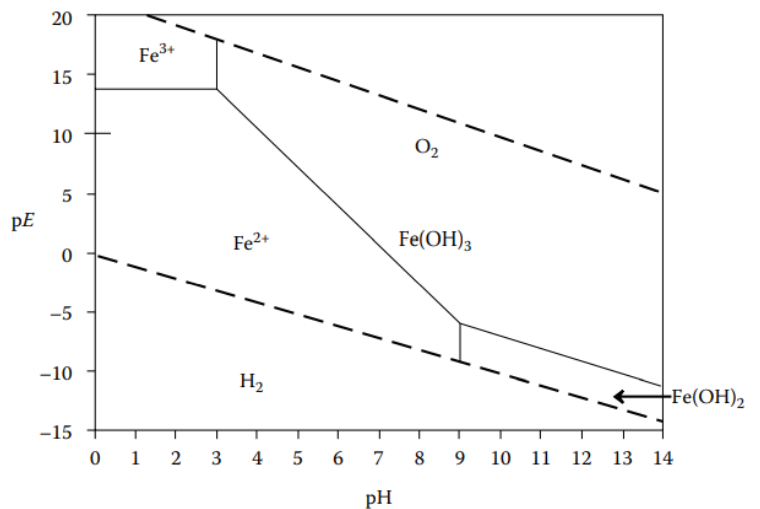


Figure 6 Simplified pE-pH diagram for soluble iron (Manahan, 2010)

is expressed in a pE-pH diagram. **FIGURE 6** shows a simplified pE-pH diagram for iron in water as an example (Manahan, 2010).

Although aquatic systems are highly dynamic and accurate pE values are difficult to obtain from electron potential field measurements, an indication of the theoretical pE can be made based on the following relation between pE, electrical potential and temperature (Pankow, 1991);

$$pE = \frac{Eh \cdot F}{2.303 \cdot R \cdot T}$$

Equation 12

With;

- Eh Electrical potential (V)
- F Faraday constant = 23061 (cal/V)
- R Gas constant = 1.987 (cal/degree)
- T Temperature (K)

Depending on the type of measurement instrument used, Eh can be seen equivalent to ORP (U.S. Environmental Protection Agency, 2013);

$$Eh (V) \cong ORP (V)$$

Equation 13

3. Methodology

The experimental setups were located in the Water Application Centre (WAC), where a groundwater well was available to deliver groundwater as feed flow. The composition of the groundwater and tap water can be found in APPENDIX I. A schematic overview of the standard setup (F01) can be seen in FIGURE 7, while APPENDIX II contains dimensions, additional photographs of both setups and a schematic of the setup used for upscaling (F02).

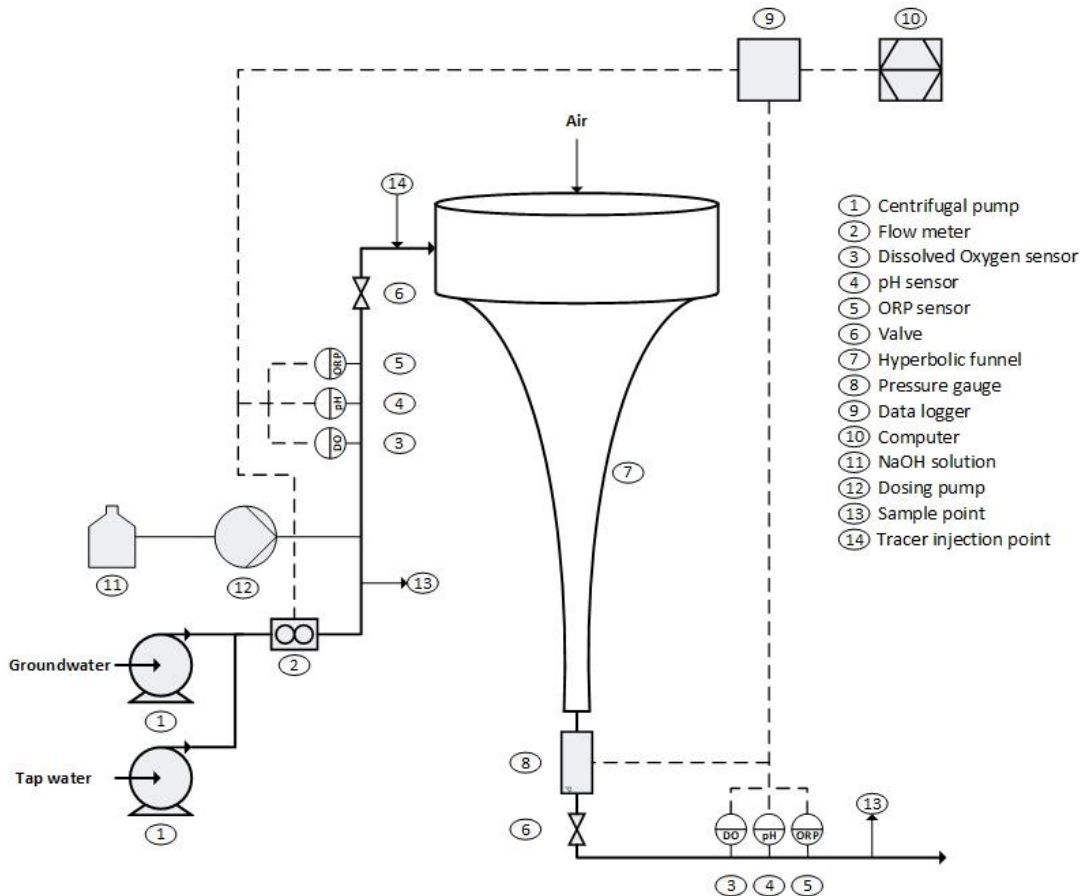


Figure 7 Schematic of setup F01

A list of all used sensors and model types can also be found in APPENDIX II. The sensors were connected to dataloggers and a laptop for collecting and storing measurements as time series. ORP-, pH and DO measurements were taken every three seconds, measurements for flow rate and pressure were taken every five seconds.

3.1 Generalization

In order to gain a better understanding of the flow behaviour within each regime, two additional flow rates were selected, representing either a boundary condition or a transition phase for a flow regime. This resulted in a total of nine flow rates to be examined for the generalization. The characteristics of the vortices were recorded and photographed for each flow rate to ensure that similar stable conditions were achieved for each repeating session. The vortex characteristics and photos

Table 1 Experimental design of system generalization

Exp.	Flow regime	Outlet restriction	Flow rate (L/min)
1.	Restricted Schaubberger	Yes	14.7
2.			15.2
3.			15.7
4.	Twisted Schaubberger	No	19.9
5.			20.4
6.			20.9
7.	Straight Schaubberger	No	22.0
8.			22.5
9.			23.0

can be found in **APPENDIX III**. An overview of the experiments can be seen in **TABLE 1**. The experiments were repeated four times.

Once a stable vortex was established, the system was operated under steady state conditions for a duration of twenty minutes for each flow rate. The steady state condition was determined based on the stabilization of DO at the outlet. The flow rate, pressure and ORP-, pH- and DO- inlet and outlet values were recorded for the duration of the experiment.

3.1.1 Tracer experiments

A tracer medium was added to the incoming stream, followed the fluid flow within the system, and was measured as the tracer exited at the outlet. These measurements were analysed for determining mean residence time, volumes and indicating mixing capacity and fluid flow within the system (Levelspiel, 2012). The pulse method was chosen for the experiments, where a short pulse of tracer medium is injected into the inlet flow, resulting in a peak in the outlet readings when the tracer leaves the system.

Sodium Hydroxide (NaOH, 1M) was selected as the tracer medium and tap water was used as feed in order to prevent consumption of the tracer due to iron oxidation. The tracer dosing point was located right before the inlet of the funnel. The vortex for a selected flow rate was stabilized similar to the generalization experiments, after which the tracer was injected on fixed time intervals of three minutes at the dosing point. This resulted in a short increase of pH measured at the outlet of the funnel. The pulses were repeated four times for all nine flow rates.

3.2 Iron oxidation

One flow rate for each regime was selected for measuring the iron oxidation under six different pH conditions, as shown in **TABLE 2**. All experiments were performed in duplicate. The selected flow regime was stabilized as mentioned in the generalization experiments, after which the pH dosing (NaOH, 1M) was started using a diaphragm liquid dosing pump (SIMDOS® 10 FEM 1.10 S). The inlet pH sensor was used to monitor pH conditions. After ten minutes of steady state conditions, water samples were collected from the inlet and outlet streams. The samples were brought to a temperature of 20 °C in a water bath before testing, as recommended by Hach® (HACH, 2013), of which the cuvette tests were used for analysis.

The concentrations of Fe²⁺, Fe³⁺ and Fe_{Tot} in the water samples were determined with the use of the Hach® cuvette test system (LCK320: iron II/III). The inlet sample was tested first, followed by the outlet sample. The minimal duration of an iron test was ten minutes and included two readings which could not be interrupted. This caused a fifteen to twenty minute waiting time before the outlet sample tests were started, due to the availability of one spectrophotometer.

Table 2 Experimental design for iron oxidation efficiency

Exp.	Flow regime	Flow rate (L/min)	pH inlet
1.	Restricted Schauburger	15.2	6.9*
2.			7.3
3.			7.7
4.			8.1
5.			8.5
6.			8.9
7.	Twisted Schauburger	20.4	6.9*
8.			7.3
9.			7.7
10.			8.1
11.			8.5
12.			8.9
13.	Straight Schauburger	22.5	6.9*
14.			7.3
15.			7.7
16.			8.1
17.			8.5
18.			8.9

* No pH control

3.2.1 Influence of contact time

The influence of this contact time on the iron concentrations was evaluated with an additional experiment, during which a TS vortex was stabilized with an inlet pH of 8.9. After steady state conditions were reached and maintained for ten minutes, nine water samples were collected at the outlet. One of the samples was tested for iron concentrations directly after collection, without use of a water bath. The remaining samples were tested after various contact times (5, 10, 20, 30, 40, 50 and 60 minutes).

3.3 Upscaling

A similar setup was used as shown in **FIGURE 7** for the larger hyperbolic funnel (F02) to evaluate upscaling, containing several adaptations. The F02 consisted of a copper cylindrical part and a hyperbolic funnel part made of fibre glass. Dimensions and a schematic can be found in **APPENDIX II**. Recirculation was applied since the groundwater pump was unable to provide the required flow rates and the drain was unable to process the high flow rate of the outlet. A cubic metre storage tank was placed next to the hyperbolic funnel from which the feed (tap water) was transported to the inlet of the funnel with a centrifugal pump. The outlet flow of the funnel was returned back to the storage tank after passing the sensor point.

For the generalization, a similar approach was taken as for F01; vortices with similar characteristics as for F01 were reproduced and stabilized for 20 minutes. During this time the flow rate and pressure were measured and determined for each flow regime. DO was not determined since the feed was not anaerobic and recirculation was applied. Tracer experiments similar to the experiments for F01 were applied for determining the HRT and V_L .

4. Results

4.1 Generalization results

The data gathered during the generalization experiments of the system showed that each flow regime can be defined based on flow rate, pressure and DO (outlet). The characteristics for each regime are summarized in **TABLE 3** and **FIGURE 8**. **APPENDIX IV** shows the data for each of the nine flow rates tested during the generalization. The overlap of the error bars seen in **FIGURE 8** between TS and SS is caused by fluctuations in flow rate by the groundwater pump, which is further discussed in **CHAPTER 5. DISCUSSION**.

Table 3 Defining parameters for each flow regime

Flow regime	Flow rate (L/min)		Pressure (millibar)		DO outlet (mg O ₂ /L)		V _{ratio} (%)		HRT (sec)	
	Min	Max	Min	Max	Min	Max	Min	Max	Min	Max
RS	14.7	15.7	68	70	0.46	0.86	44	82	21	37
TS	19.9	20.9	-1.1	2.5	1.30	1.84	39	65	14	22
SS	22.0	23.0	5.2	6.8	1.17	1.24	91	95	29	30

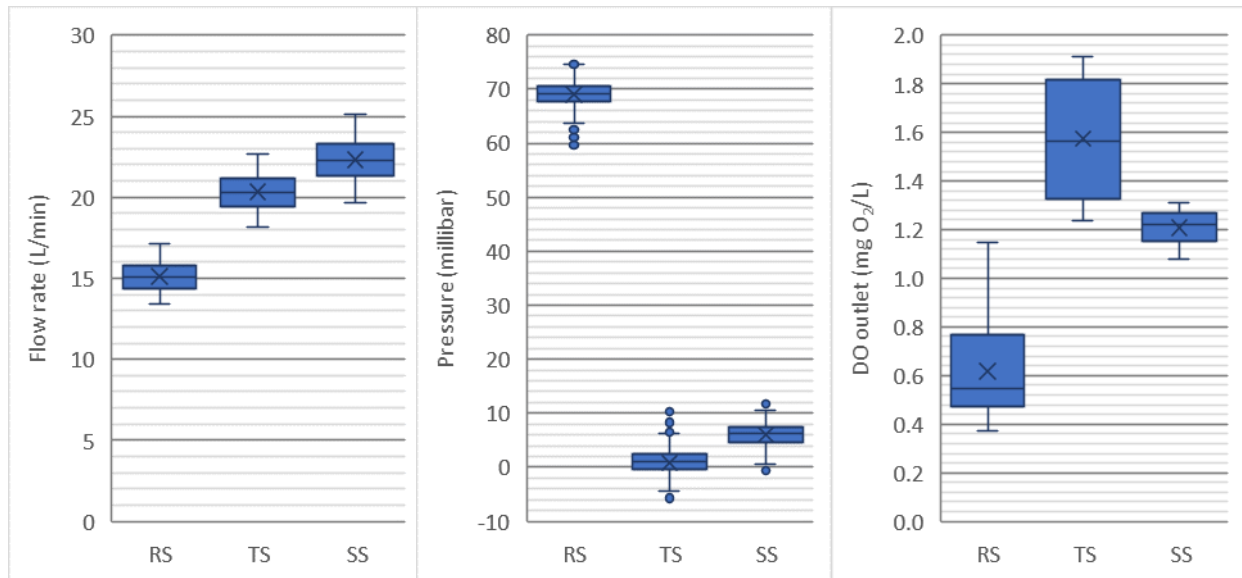


Figure 8 Flow rates, pressure and DO values for each flow regime

Based on the dimensions of the hyperbolic and cylindrical parts of the funnel, the total volume (V_T) was calculated to be approximately 11.7 L. Visual analysis and calculation were used to acquire a first indication for the liquid volume present in the funnel for each flow rate. V_{ratio} represents the portion of the funnel that is occupied by liquid. All calculations for volumes and HRT can be found in **APPENDIX V**. The calculated volumes and flow rates were used to provide a first indication of the HRT in each regime. These values were further verified using tracer experiments.

The results show that the TS provides the greatest DO increase of the three flow regimes within a very short HRT of 14 to 22 seconds, especially in the lower flow rates. This can be linked to the wide, helically shaped vortex that is formed, which provides a large area-to-volume ratio; one of the key factors for efficient aeration. Similarly, the RS is the flow regime with the smallest air-water interface, forming a short and narrow vortex, showing the lowest DO increase of the flow regimes. The increase in pressure seen in the RS is created by the restriction applied at the outlet, which, in contrast to the other two flow regimes, is necessary to form the RS vortex.

4.1.1 Tracer experiment results

The collected data for the outlet pH during the tracer experiments was converted to concentration (C_{NaOH}) and expressed in mg/L. The constant pH of the feed before the pulse was subtracted from each data point, resulting in the increase in concentration compared to the constant pH of the feed. Graphing C_{NaOH} over time resulted in the mean residence time distribution curve (RTD-curve) for each pulse. The RTD-curves showed a distinctive peak for each flow rate and flow regime (see APPENDIX VI for graphs and calculations). FIGURE 9 shows a comparison of peaks representative for each flow regime.

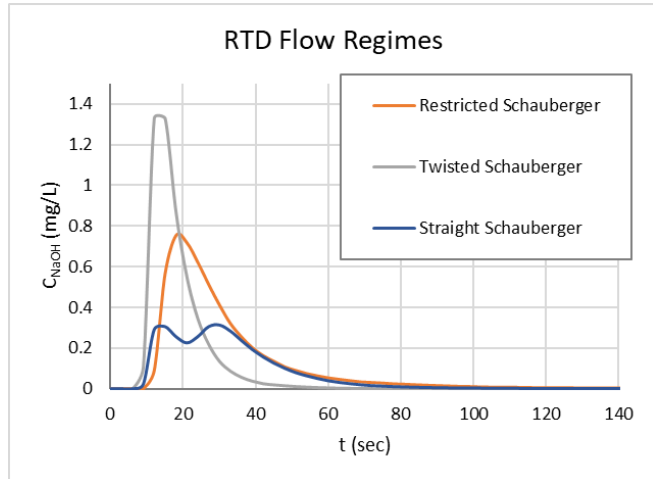


Figure 9 Mean Residence Time Distribution (RTD) curves representative for each flow regime

The mean residence time and water volume were calculated for each pulse based on the gathered data (see APPENDIX VI for calculations). The ratio between the total reactor volume (V_T) and the water volume according to the tracer experiments (V_{Tracer}) can be used to provide additional information about the fluid flow in the following way;

$$\frac{V_{\text{Tracer}}}{V_T} \cong 1, \text{ whole system active}$$

$$\frac{V_{\text{Tracer}}}{V_T} < 1, \text{ indication of dead spaces or stagnancy}$$

$$\frac{V_{\text{Tracer}}}{V_T} > 1, \text{ indication of a measurement error}$$

These results can be found in TABLE 4 and FIGURE 10. For the majority of the flow rates V_{Tracer} is smaller than V_T , indicating dead or stagnant volume present in the system. This can be justified by the gas phase present in the funnel, as shown by the similarities of V_{Tracer}/V_T and V_{Ratio} in TABLE 3.

Table 4 Results of the tracer experiments for each flow regime of the hyperbolic funnel

Flow regime	Flow rate (L/min)	HRT _{Tracer} (sec)	V _{Tracer} (L)	V _{Tracer} / V _T (-)
RS	RS1	14.7	24	0.51
	RS2	15.2	32	0.70
	RS3	15.7	36	0.81
TS	TS1	19.9	13	0.38
	TS2	20.4	19	0.54
	TS3	20.9	23	0.69
SS	SS1	22.0	29	0.90
	SS2	22.5	31	1.01
	SS3	23.0	32	1.04

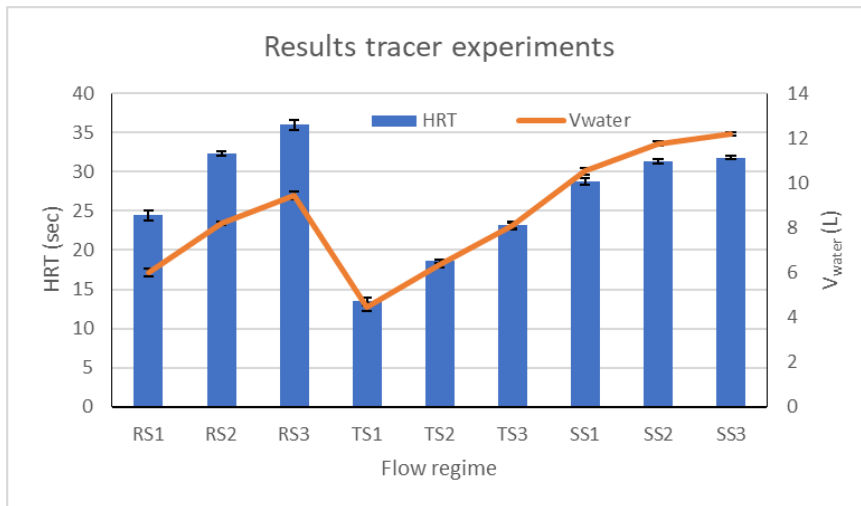


Figure 10 HRT and liquid volume according to the data acquired with tracer experiments

For further analysis of the fluid flow, the RTD-curves were converted into E_{θ} -curves, where both the x- and y-axis are dimensionless and the area under the curve equals to 1. FIGURE 11 shows the different E_{θ} -curves obtained for each regime. The calculations and E_{θ} -curves for all flow rates can be found in APPENDIX VI. The main objective of the E_{θ} -curves is fitting the system to flow models.

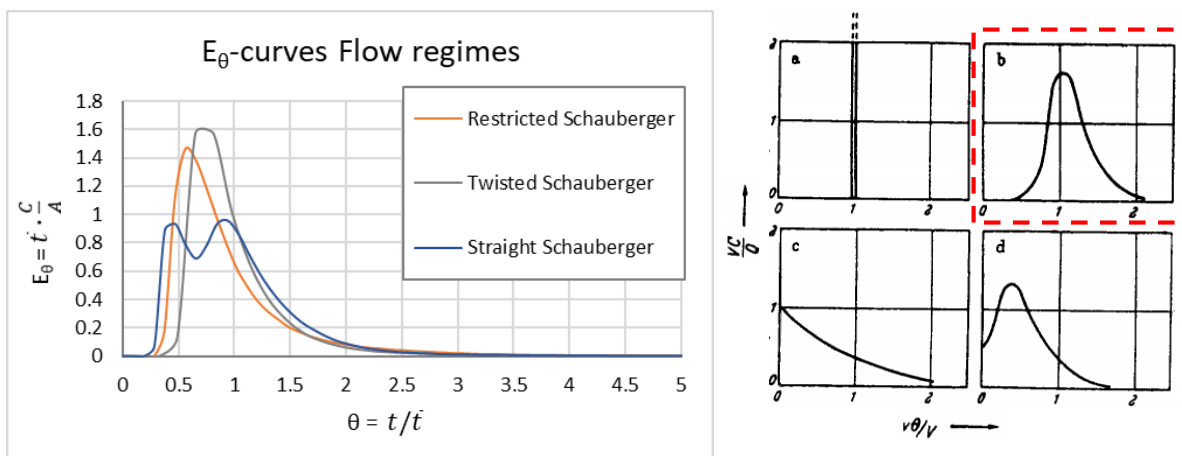


Figure 11 On the left: E_{θ} -curves representative for each flow regime of the hyperbolic funnel. On the right: diagrams for (a) plug flow; (b) plug flow with longitudinal mixing; (c) complete mixing (CSTR) and (d) dead water (Danckwerts, 1953).

From the obtained shapes of the curves, it can be concluded that the hyperbolic funnel is comparable to a plug-flow reactor with longitudinal mixing (Danckwerts, 1953) (Hoeben, 2021). The deviation from plug flow due to internal mixing can be expressed by the Dispersion number (D/uL), where $D/uL < 0.01$ means a small deviation from plug flow and $1 > D/uL > 0.01$ means a large deviation from plug flow (Levelspiel, 2012). When comparing the curves from the hyperbolic funnel with response curves for several Dispersion numbers for closed-closed boundary conditions (see APPENDIX VI), it can be seen that D/uL varies from 0.02 to 0.1, depending on the flow regime and flow rate. This indicates a large deviation from plug flow, meaning rapid mixing of the liquid phase.

Comparing the HRT and volumes obtained in the generalization and in the tracer experiments, it can be concluded that most of the results from both methods show good correspondence. The HRT often deviates not more than one second and the volume not more than 5%, except for RS1, SS2, and SS3. In case of RS1 this might be due to the fact that the vortex does not follow the hyperbolic function in this case, resulting in a deviation of the liquid volume and HRT. In case of SS2 and SS3, the double peak

that is seen in the curves for these two flow rates indicate a parallel flow pattern, most likely due to channeling (Levelspiel, 2012) (Hoeben, 2021). Here the first and second peak represent the fast and slow flowing fluids accordingly. Even though the HRT are quite similar to the calculated values for SS1 and SS2, it is indicated that the liquid volumes are higher than the total volume of the hyperbolic funnel. This might be due to a reaction between the tracer and the vessel wall, in this case the material of the top lid, resulting in a delay of the tracer passing through the system and a shift in the mean residence time, therefore also resulting in a liquid volume that is too high. This is also indicated by the V_{Tracer}/V_T ratio, which is slightly bigger than 1 (indication of a measurement error, (Levelspiel, 2012)).

4.1.2 Aeration efficiency results

The aeration efficiency was determined for each flow rate, based on the results from the generalization experiments. Firstly, the K_La was calculated according to equation 5, where the DO concentration at the outlet (C_L) was adjusted to account for the DO consumption due to iron oxidation (see paragraph 2.3.1 VOLUMETRIC MASS TRANSFER COEFFICIENT (KLA) and CHAPTER 5. DISCUSSION). Next, the K_La was normalized for a water temperature of 20 °C, resulting in the K_{La20} (Equation 6). With K_{La20} now known, the SOTR of the system was calculated for each flow rate with Equation 8. Lastly, the SAE was calculated with Equation 9.

The resulting K_La and SOTR for each flow regime and flow rate are presented in TABLE 5 and FIGURE 12. The V_L used for the calculations were derived from the average of the results from the tracer experiments and the calculated values, with the exception of the two highest flow rates (SS1 and SS2). These flow rates showed a higher V_L during the tracer experiments than V_T and were therefore considered deviating. The calculated V_L were used for these two flow rates instead.

Table 5 K_La , SOTR and SAE values for several flow rates in each flow regime for the hyperbolic funnel

Flow regime	Flow rate (L/min)	K_La (T = 13 °C) (h ⁻¹)	K_{La20} (h ⁻¹)	SOTR (kg O ₂ /h)
RS	RS1	14.7	13.8	0.14
	RS2	15.2	6.0	0.06
	RS3	15.7	4.7	0.05
TS	TS1	19.9	52.5	0.67
	TS2	20.4	32.8	0.42
	TS3	20.9	21.8	0.29
SS	SS1	22.0	16.0	0.22
	SS2	22.5	15.5	0.22
	SS3	23.0	15.1	0.22

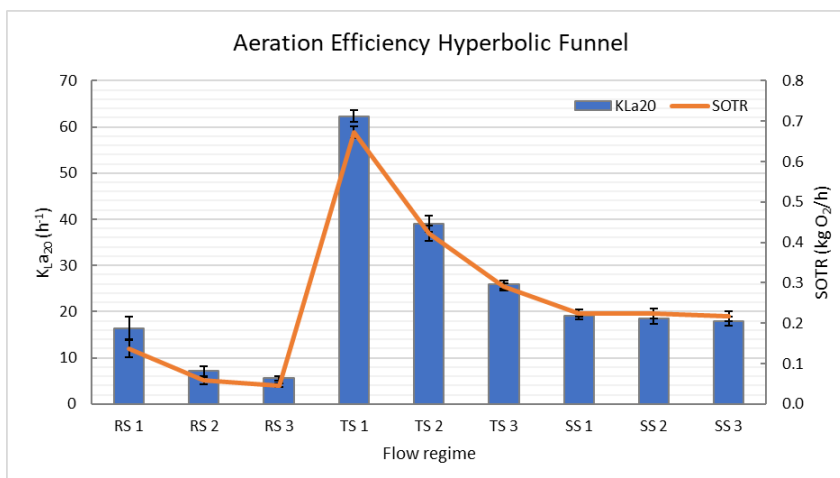


Figure 12 Aeration efficiency in terms of K_{La20} and SOTR for the hyperbolic funnel

The TS clearly shows the highest aeration capacity of the flow regimes, especially at lower flow rates. A possible explanation could be a favourable area to volume ratio within this regime, providing both a large interface (diffusion) and sufficient volume where secondary flow patterns can arise (mixing of bulk liquid). The mass balance (Equation 1) in paragraph 2.2 AERATION AND GAS TRANSFER shows that these two factors are highly influential for the gas transfer within a system. The RS shows the lowest aeration capacity, which is also the regime with the smallest air-water interface. When comparing the hyperbolic funnel to other aeration systems, it can be seen that the K_{La} is much higher (TABLE 6), especially for the TS.

Table 6 Comparison of aeration efficiency of the hyperbolic funnel and other aeration methods

Aeration method	K_{La20} (h^{-1})	SAE ($kg\ O_2/kWh$)	Reference
Curved blade rotor (CBR) (mechanical)	4.15 – 11.5	1.17 – 2.27	(Thakre, Bhuyar, & Deshmukh, 2008)
Brush rotor (mechanical)	1.61 – 2.94	1.52 – 2.13	(Thakre, Bhuyar, & Deshmukh, 2008)
Coarse Bubble (diffused)	0.44 – 1	1.22 – 2.13	(Song, 2019), (Environmental Dynamics International, 2017)
Fine Bubble (diffused)	1.64	2.43 – 7.3	(Song, 2019), (Environmental Dynamics International, 2017)
Cascade	4.89	-	(Thacker, Katkar, & Rudra, 2002)
Vortex impeller	0.71 – 37.09	-	(Warrener, 2020)
Hyperbolic funnel	5.1 – 62.3	1.9 – 23.1	-

The power requirements P used for calculating the SAE for the hyperbolic funnel were based on the previous work of Nicolae Şişcanu, where recirculation was applied for operating the funnel (Şişcanu, 2020). This power is therefore based on the potential energy due to elevation difference and inlet restriction. In case of larger elevations and restrictions, a higher power consumption would be required, which would have a large influence on the SAE that is shown here. Another factor to keep in mind is that the SOTR is based on an oxygen increase from 0-2 mg/L in the funnel and not from 0 to saturation, which could result in a more optimistic outcome of the SOTR. These factors make that the SAE as shown in TABLE 6 should be considered as a theoretical maximum, and both factors are further discussed in CHAPTER 5. DISCUSSION.

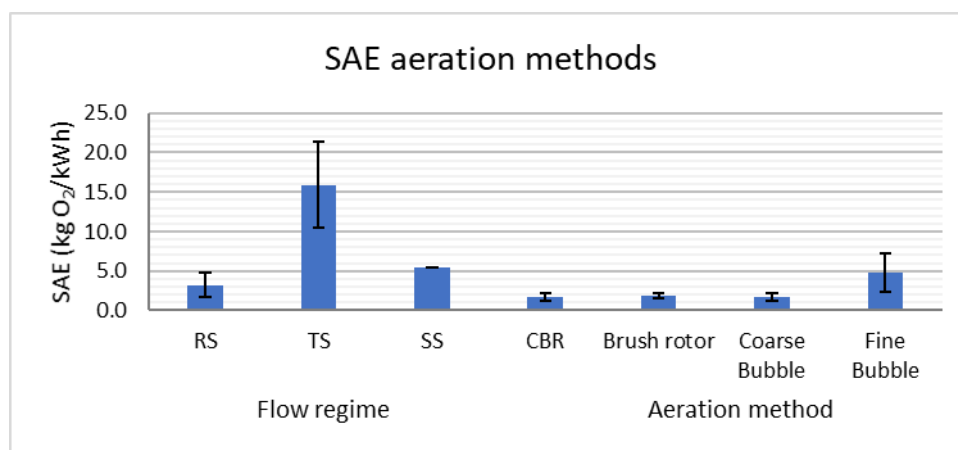


Figure 13 Comparison of SAE for flow regimes of the hyperbolic funnel and other aeration methods.

A comparison of the SAE for this particular scenario with other methods is presented in FIGURE 13. Here it can be seen that the RS and SS regimes are comparable with other aeration methods, fine bubble aeration in particular. The TS regime shows a SAE higher than the other regimes and aeration methods. This is largely assigned to the high aeration efficiency (K_{La}) in this regime and corresponds to the

expectations of the efficiency of the system. However, it should be kept in mind that the SAE is heavily influenced by both pump requirements and SOTR, and that further research and calculations are necessary for verifying the SAE for a more reliable comparison, as will be discussed later in this report.

4.2 Iron oxidation results

The measured concentrations of Fe^{2+} , Fe^{3+} and Fe_{Tot} for each experiment can be found in **APPENDIX VII**. The iron oxidation efficiency was determined using Equation 14;

$$\eta_{iron\ ox.}(\%) = \left(\frac{[Fe_{in}^{2+}] - [Fe_{out}^{2+}]}{[Fe_{in}^{2+}]} \right)$$

Equation 14

These efficiencies were based on a twenty minute contact time for the outlet sample and were corrected for time $t = 0$ minutes. According to the results of the contact time experiment (**3.2.1 INFLUENCE OF CONTACT TIME**), the iron oxidation efficiency increases with approximately 45% from $t = 0$ to $t = 20$ minutes (**FIGURE 14**).

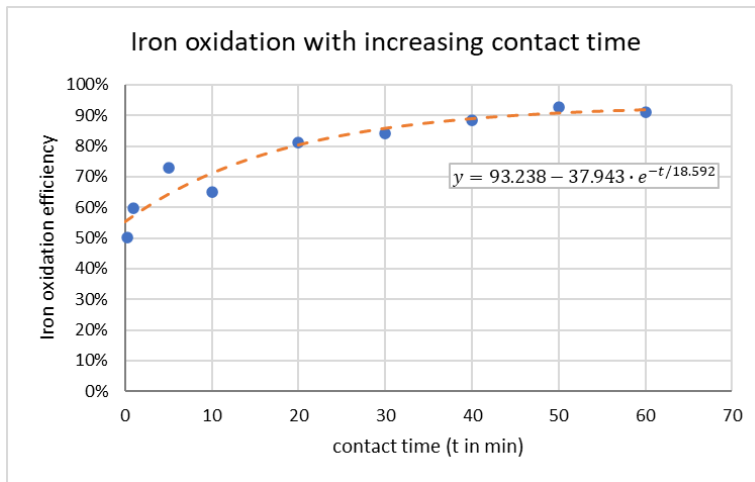


Figure 14 Influence of time on the iron oxidation efficiency in the TS (pH 8.9)

Based on this influence of contact time, the calculated iron oxidation efficiencies were extrapolated to produce iron oxidation efficiencies at time $t = 0$, which can be seen in **TABLE 7** and **FIGURE 15**.

Table 7 Iron oxidation efficiency of the hyperbolic funnel with each flow regime under various pH conditions

Flow regime	Flow rate (L/min)	Iron oxidation (t = 0 min.)					
		pH 6.9	pH 7.3	pH 7.7	pH 8.1	pH 8.5	pH 8.9
RS	15.2	3.4%	4.0%	4.5%	4.5%	9.2%	26.7%
TS	20.4	6.3%	7.8%	9.3%	12.5%	18.5%	55.8%
SS	22.8	4.7%	6.2%	6.5%	7.7%	11.3%	34.7%

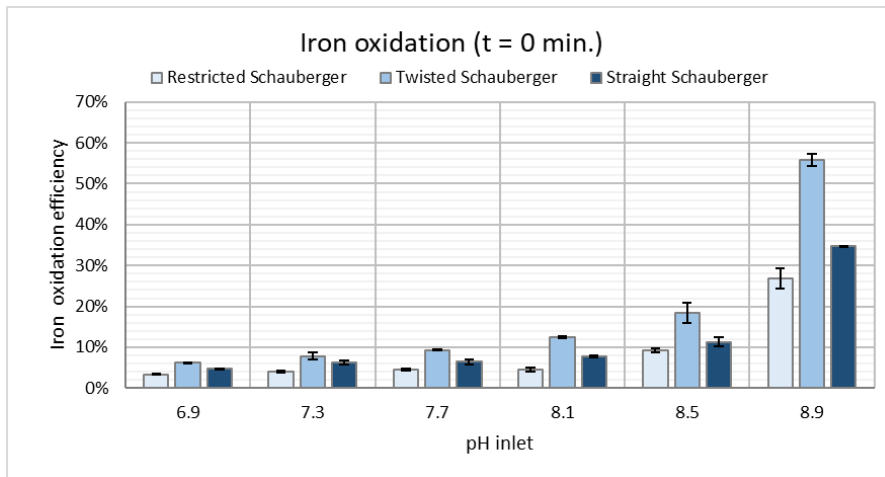


Figure 15 Overview of the iron oxidation efficiencies for each flow regime under various pH conditions

The TS shows the highest iron oxidation efficiency in all pH conditions. The iron oxidation increases with increasing pH, with the largest increase from a pH of ≥ 8.5 , which is the point where NaOH is dosed in excess. This can be seen in the clear increase in the outlet pH as well as the inlet (see APPENDIX VII). The highest iron oxidation efficiency is reached in the TS with a pH of 8.9, reaching 55.8% at time $t = 0$. However, as presented in FIGURE 14, the DO concentration in that case was already enough to reach 90% efficiency, nevertheless only after 50-60 minutes contact time. In real water treatment processes this can be achieved by using slow mixing or contact basins.

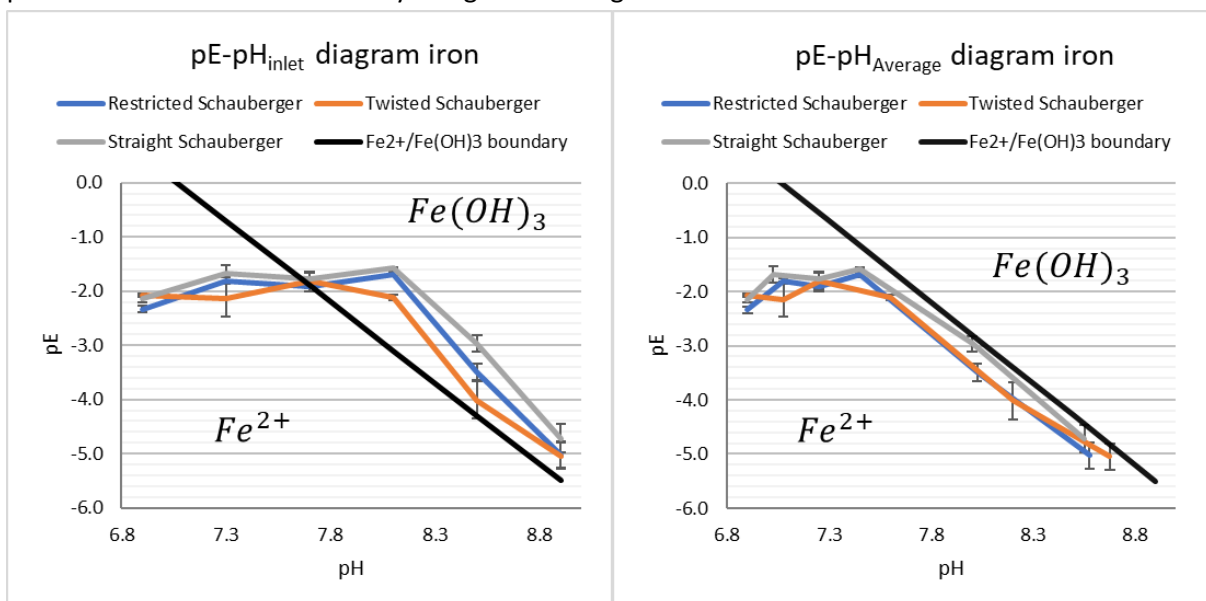


Figure 16 Implementation of experimental data in a pE-pH diagram of the aquatic conditions within the hyperbolic funnel during the iron oxidation experiments (Manahan, 2010).

The data for the iron oxidation experiments were implemented in pE-pH diagrams (FIGURE 16), from which the left graph was based on the inlet pH only and the right graph on the average pH of inlet and outlet. It shows that the iron oxidation in the hyperbolic funnel takes place closely around the pE-pH boundary between Fe^{2+} and $Fe(OH)_3$ formation (FIGURE 6), especially during the two highest pH conditions selected for the experiments. It can also be seen that the NaOH dosing causes a lowering in pE in these conditions, impeding the oxidation of Fe^{2+} at pH conditions ≥ 7.8 . When looking at the iron oxidation efficiencies, it is expected that the $Fe^{2+}/Fe(OH)_3$ boundary is only clearly crossed in the hyperbolic funnel under pH (inlet) conditions of ≥ 8.5 . This is further confirmed by graphing the logarithm of the equilibrium constant K for the reaction of iron oxidation for each tested pH condition.

Only at the highest pH condition does the log K exceed 0, indicating that the formation of products ($\text{Fe}^{3+} \rightarrow \text{Fe}(\text{OH})_3$) is favoured (FIGURE 17).

TABLE 8 shows a comparison with other aeration systems used for iron oxidation. The efficiencies shown in the table are after aeration and before filtration, similar to the hyperbolic funnel. Although the hyperbolic funnel seems less efficient than most methods presented in the table, the differences in HRT have to be considered. The diffused aeration methods often mention longer aeration times, varying from fifteen minutes up to five hours, while the vortex impeller reports HRT of 8-56 minutes. Krupinska (2017) also mentions two hours of sedimentation between fifteen minutes of aeration and the iron determination. The hyperbolic funnel on the other hand reaches the stated oxidation efficiency within a HRT of less than half a minute. When considering additional contact time after sample collection of the hyperbolic funnel, it is shown that iron oxidation efficiencies of 80-90% can be reached within twenty to sixty minutes, which would be similar or higher than the other aeration methods. This is achieved however with a higher pH condition compared to the other methods.

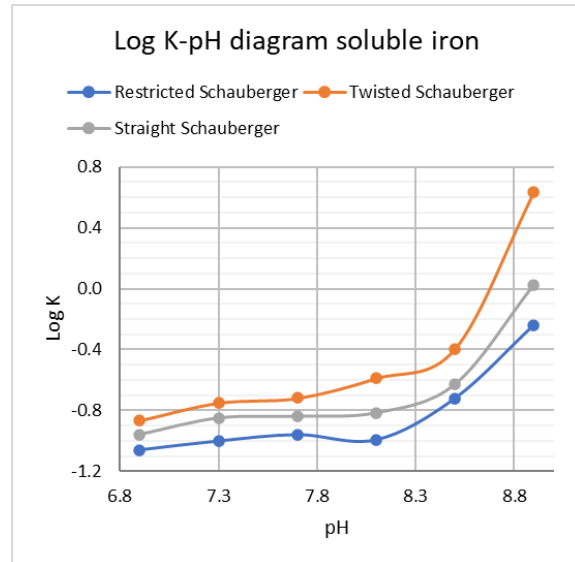


Figure 17 Log K-pH diagram for soluble iron during the iron oxidation experiments, with $K = \frac{[\text{Fe}^{3+}]}{[\text{Fe}^{2+}]}$.

Table 8 Comparison of iron oxidation efficiency for the hyperbolic funnel and other aeration systems

Aeration method	Fe^{2+} inlet (mg/L)	pH	Iron oxidation efficiency (%)	Reference
Diffused	3.39	6.97 – 7.14	88 – 95	(Krupinska, 2017)
Diffused	-	6	66 – 72	(Paul, Vijayan, Raju, Megha, & Sadique, 2016)
Diffused	0.65	8.39 – 8.51	14 – 39	(Marjani, Nazari, & Seyyed, 2009)
Cascade	0.85	6.4	49	(Siabi, 2008)
Cascade	1.8	7.6	70 – 85	(Sharma, 2001)
Vortex impeller	4.6	6.9 – 8.1	15 – 83	(Warrener, 2020)
Hyperbolic funnel	4.6	6.9 – 8.9	3.4 – 55.8	-

4.3 Upscaling results

The generalization was repeated with setup F02 in order to gather the defining parameters regarding the flow regimes in the large funnel. A comparison between the small and large funnel of the defining parameters is shown in TABLE 9, where F01 represents the small funnel and F02 the large funnel. V_L and HRT were determined with tracer experiments, since the material of the funnel did not allow calculation based on visual analysis. The volume was validated by the difference in water volume present in the buffer tank once each vortex was stabilized. The inlet velocity (v_i in m/s) was calculated with Equation 15, where Q is in m^3/s and A is the area of the inlet in m^2 ;

$$v_i = \frac{Q}{A}$$

Equation 15

The angular velocity (ω) was then calculated with Equation 16, where $r_{cylinder}$ is the radius of the cylindrical part or the funnel;

$$\omega = \frac{v_i}{r_{cylinder}}$$

Equation 16

Table 9 Comparison of defining parameters per flow regime of F01 and F02

Flow regime		Flow rate (L/min)		Inlet velocity (m/s)		Angular velocity (rad/s)		Pressure (millibar)		V _{ratio} (%)		HRT (sec)	
		F01	F02	F01	F02	F01	F02	F01	F02	F01	F02	F01	F02
RS	Min	14.7	44	1.08	1.04	7.18	3.46	69	108	44	43	21	57
	Max	15.7	49	1.14	1.16	7.62	3.85	70	110	82	53	37	64
TS	Min	19.9	65	1.46	1.53	9.73	5.11	-1.1	-0.5	39	22	14	20
	Max	20.9	77	1.52	1.82	10.2	6.05	2.5	19	65	46	22	35
(SS1)		22.0	78	1.60	1.84	10.7	6.13	5.2	20	91	61	29	46
SS	Min	22.5	90	1.64	2.12	10.9	7.07	6.1	21	94	95	29	57
	Max	23.0	100	1.67	2.36	11.2	7.86	6.8	35	95	96	30	62

No immediate coherence was found between the two systems, possibly due to differences in geometric ratios (C-constant) and material. This can be seen by the decreasing difference in angular velocity with increasing flow rate, indicating more friction has to be overcome in F02 for the formation of comparable vortices. It can also be seen that SS1 shows the most deviations. This can be linked to the fact that SS1 represents a transition phase between TS and SS, which shows more similarities to SS in F01 and towards TS in F02. These points are elaborated further in **CHAPTER 5. DISCUSSION**.

Regarding the curves of the tracer experiments for F02, it can be seen that they are similar to F01, indicating comparable flow behaviour in both systems (**FIGURE 18**). The peaks for RS and SS in the E_{θ} -curve are earlier for F02. Looking at **FIGURE 11**, this can be an indication for more dead spaces present in the liquid phase compared to F01.

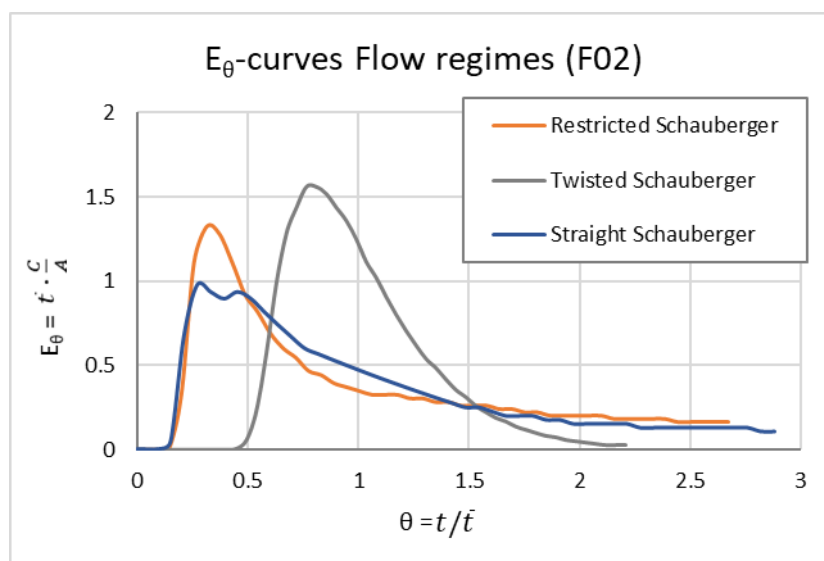


Figure 18 E curve representative for each flow regime of F02

For predicting the formation of a certain regime in a given system, a non-dimensional number can be proposed based on funnel geometry (\emptyset in- and outlet, \emptyset cylinder, height hyperbolic, C-constant), flow characteristics (flow rate, (angular) velocity) and fluid- and material properties (density, viscosity, surface tension, friction). However, it was found that extended research containing a variety of systems is needed to compose and validate the use of a non-dimensional number.

5. Discussion

Pump fluctuations

The groundwater pump worked based on maintaining a certain pressure; if the pressure would drop too low, the pump would start up until the desired pressure was achieved, then shut down again. The pump would repeat this cycle to maintain the pressure. This meant that the flow rate delivered to the system would fluctuate with 2.5 (RS) to 4 (SS) L/min between the pump starting and shutting down. The mean flow rate of the pump was stable however. To account for these fluctuations, the flow meter was logged and the calculated mean for the duration of each experiment was applied as the flow rate. These pump fluctuations can be recognized in **FIGURE 8**, giving larger error bars for the characteristic parameters. The fluctuations did not largely influence the mean values for the parameter. It is expected, that with a pump delivering a more stable flow rate, the range of the measured parameter would be closer to the mean values since the system would be in a more stable condition.

Volume determination

The determination of V_L during a certain regime based on visual analysis presented some challenges. Firstly, the refraction caused by the glass due to the shape and the elongated size of the system made it difficult to produce images on which the vortex (and therefore the interface) was recorded correctly (see photographs in **APPENDIX IV**). Due to time limitations it was chosen to calculate the liquid volume instead, based on the assumption that the vortices would follow the hyperbolic function $f(x) = \frac{1}{x}$. This assumption was supported by the tracer experiments, giving largely similar results.

However, a computational analysis of the interface would produce more precise results because it would also consider the additional interface area created by the helical shape observed in the vortices. Another advantage would be the determination of the area of the interfaces. Then the ratio between volume and interface area within the system can be given, which is an important parameter for aeration systems (See **2.3.1 VOLUMETRIC MASS TRANSFER COEFFICIENT (K_LA)**).

Sample collection

Due to the anaerobic nature of the groundwater it was important to minimize air contact during sample collection as much as possible to produce representable results. Collecting the samples in a collection vessel (e.g. a centrifuge tube) already caused fluctuations in iron measurements, even when filling the entire vessel. This effect was minimized when using syringes for sample collection and sealing the nozzle with parafilm, providing repeatable iron results. This does however show the sensitivity of sample collection for the iron measurements.

Another factor that influenced the iron measurements was the time between sample collection and measurement. For the outlet samples this was twenty minutes, for which the iron oxidation efficiencies were corrected based on the result of the contact time experiment. This extrapolation does however add an uncertainty to the iron oxidation efficiencies at time $t = 0$.

Aeration efficiency

Officially the SOTR is stated to be determined with clean (tap) water, with a DO concentration of 0 mg/L at a temperature of 20 °C and atmospheric pressure (European Standards, 2004). All requirements for the calculation of the aeration efficiency are met during this research, with the exception that groundwater was used instead of tap water. The presence of iron in this feed may influence the aeration efficiency calculations due to chemical reactions (see **2.3.1 VOLUMETRIC MASS TRANSFER COEFFICIENT (K_LA)** and **2.4.1 HOMOGENOUS OXIDATION**). The influence of this iron oxidation was accounted for based on stoichiometry and an oxygen mass balance, which showed only small

deviations ($\pm 4.5\%$) from the original calculated K_{La} . Tests performed by Nicolae Şişcanu where tap water was used as feed also showed very similar K_{La} values (Şişcanu, 2020). Therefore it was assumed that the usage of groundwater as a feed does not have a large influence on the SOTR.

The SAE on the other hand is highly dependent on both pump requirements and SOTR. For this research, the pump requirements were based on the tests performed by Nicolae Şişcanu, where recirculation was applied to the system. However, if a larger elevation, distance or inlet restrictions are to be overcome, a larger P is required. This has a large impact on the SAE, since SAE is inversely proportional to the power consumption. The same applies to the SOTR; as mentioned before, this coefficient was based on an oxygen increase from 0-2 mg/L and not from 0 to saturation. Due to the exponential behaviour of the oxygen transfer rate, this means that the SOTR is based on the part of the curve where the oxygen transfer rate is highest, possibly resulting in a more optimistic outcome. Both mentioned factors resulted in high SAE values, especially for the TS regime.

Tracer experiments

Overall, the tracer experiments showed results that matched up very well with the calculations based on visual interpretation. However, the two highest flow rates in the SS regime deviated; they showed a higher liquid volume than the total volume of the funnel itself. It was assumed that this was caused by reaction of the tracer with the top lid material, since the two highest flow rates are the only two that reach the lid.

Another assumption was that the used tracer would be close to inert when using tap water as feed. This was supported by similar HRT acquired by both the tracer experiments and the calculations and were acknowledged by dr.ir. Wilfred Hoeben, professor at Eindhoven University of Technology (Hoeben, 2021). The tracer was also tested with groundwater as feed, which is highly reactive with the tracer as a comparison. This showed that due to the reaction between tracer and groundwater, no HRT higher than fifteen seconds could be measured before the tracer was consumed.

Upscaling

An important difference in geometry of both systems is the C-constant, which gives the sharpness of the hyperbolic curve; this C-constant is larger for F02, resulting in a steeper decline in diameter along the hyperbolic part compared to F01. Another difference between the two systems was the material (glass and copper/fiber glass), resulting in differences in friction at the vessel wall. These two points imposed difficulties in acquiring comparable vortices in both systems, resulting also in datasets that were difficult to compare.

Another factor that added to this was the level meter applied for acquiring the water level in the funnel. The combination of high flow rate and the accuracy of the meter complicated the collection of precise measurements, therefore impeding the determination of the flow conditions that result in comparable filling ratios opposed to F01. This can be seen in some differences of V_{ratio} between both systems, for instance at RS max, TS min and SS1. This further impeded the formation of similar vortices in both systems for comparison and the formation of a non-dimensional number.

6. Conclusion

During the generalization of the hyperbolic funnel it was observed that each flow regime can be characterized based on flow rate, pressure and DO uptake. By using tracer technology it has been found that the system is comparable to a plug-flow reactor with longitudinal mixing. The TS showed the highest aeration capabilities of the regimes, with K_La values of 25-62 h^{-1} . When looking at the aeration coefficients (K_La , SOTR and SAE), the TS outperforms other aeration methods, the K_La in particular. However, further research and/or numerical studies are needed for acquiring a more accurate SOTR and SAE for a more reliable comparison to other aeration methods.

The TS also showed the highest iron oxidation efficiencies of all regimes, followed by the SS and RS subsequently. With increasing pH, the iron oxidation efficiencies increased as well, while maintaining the same order among the flow regimes within each pH condition. The highest iron oxidation efficiency was achieved with the TS and pH conditions of 8.5 and 8.9 (18.5-55.8% respectively). By increasing the contact time after aeration by 20-60 minutes, iron oxidation efficiencies of up to 80-90% could be achieved. When comparing this to other aeration methods, the hyperbolic funnel shows similar to higher iron oxidation efficiencies. However, higher pH conditions were applied to achieve this, partially due to the reducing nature of the applied dosing agent, resulting in more chemical usage for pH control.

When applying upscaling, little coherency was found between the defining parameters of both funnels due to differences in geometry and material, impeding the formation of a non-dimensional number. Tracer experiments show similar flow behaviour in both systems, with the addition that more dead spaces in the liquid seem to be present in the RS and SS of the larger funnel.

Is the Hyperbolic vortex suitable as an alternative aeration method for iron oxidation in groundwater?

The results show that the hyperbolic funnel reaches promising aeration efficiencies compared to other aeration methods, especially in the TS regime. This regime shows high K_La and SAE values, indicating that the system possesses large oxygen transfer capabilities with lower energy requirements, making it a suitable and more sustainable alternative for aeration. However, this is based on a single bench scale setup and more research is required in order to evaluate and compare the system to other methods on a larger (industrial) scale, especially for the SOTR and SAE coefficients.

When applying the hyperbolic funnel for iron oxidation in groundwater, it is capable of reaching similar to higher iron oxidation efficiencies than other methods, while maintaining a short HRT in comparison. This shows that the hyperbolic funnel can be a suitable alternative aeration method when applied for iron oxidation in groundwater. The iron oxidation process can be optimized further by extending aeration and/or contact time after aeration and a well-considered selection of the applied pH-dosing chemical, so that pH-dosing (e.g. chemical usage) can be minimized.

7. Recommendations

Oxidation is only one of many applications for aeration systems. It is therefore recommended to explore more possible applications for the hyperbolic funnel. This research however focussed on iron oxidation, and therefore the overall recommendations based on the acquired results consist of further research in optimizing the system, both in generalization as well as in iron oxidation;

Generalization

➤ **Tracer experiments from the gas phase**

Only the liquid flow was evaluated during the tracer experiments in this research. The funnel is a two-phase system however, and performing the tracer experiments in the gas-phase would complement this further (e.g. diffusion behaviour of oxygen). A possible approach could be to provide an inert gas phase (e.g. N₂) and add O₂ in pulses as the tracer.

➤ **Assessment of the interface areas**

By determining the precise interface area, for instance with modelling or computational analysis, the ratio between liquid volume and interface area can be acquired. This is an important parameter for evaluating aeration systems, since K_{La} can also be expressed as $K_L \cdot (A/V)$.

➤ **Optimized gas transfer**

The gas phase consisted of air during this research, meaning that only about 20% of the gas phase consisted of oxygen available for oxygen transfer. An interesting experiment would be to increase the concentration of oxygen in the gas phase and measure the effects on the outlet DO concentration. Since 20% of O₂ provides 1.8 mg DO/L, 100% O₂ could in theory reach higher DO concentration.

➤ **Verification SAE**

Further testing and calculations are required for verification of the SAE. For instance by determining the SOTR based on a DO uptake from 0 to saturation and for a variety of systems, either experimentally (system in series/recirculation) or by numerical study (extrapolation). A similar approach can be used for determination of the power consumption.

Upscaling

➤ **Performance of upscaled funnel**

The possibilities for upscaling should be further evaluated in terms of performance and non-dimensionalization. More extensive research of a variety of systems is required to provide more comparable data to which a non-dimensional number can be fitted and validated (e.g. apply variations either in size or in materials, while maintaining geometry). In terms of the performance, at least the aeration efficiencies should also be determined for an upscaled funnel. By comparing these efficiencies with the glass funnel, it can be evaluated if upscaling is a useful approach or if performance in series would be more suitable for larger scale applications.

Iron oxidation

➤ **Increased aeration time and/or contact time**

Increasing the aeration time might influence the iron oxidation efficiency of the system, while additional contact time showed an increase in iron oxidation efficiency. The aeration time could be prolonged by for instance operating hyperbolic funnels in series. The contact time can be prolonged by adding a sedimentation or slow flow basin to the system. These two factors

might contribute to optimizing the pH dosing by raising the pE and/or allowing more time for the oxidation to take place, so that more neutral pH conditions might be applied.

➤ **Selection pH-dosing agent**

Further optimization could be done by selecting a more suitable pH-dosing agent that induces less or no decrease in pE, so that iron oxidation takes place under more neutral pH conditions and chemical usage can be minimized. Further gains for sustainability can be made by searching for green chemicals as an alternative pH-dosing agent.

References

- Anastas, P. T., & Warner, J. C. (1998). *Green Chemistry: Theory and Practice*. New York: Oxford University Press.
- Anestas, P. T., & Zimmerman, J. B. (2003). Design through the Twelve Principles of Green Engineering. *Env. Sci. Tech.*, 37(5), 94-101.
- B.C. Groundwater Association. (2007, 02). *Water Stewardship Information Series: Iron & Manganese in Groundwater*. Retrieved from Regional District of Nanaimo: <https://www.rdn.bc.ca/cms/wpattachments/wpID2284atID3808.pdf>
- Benjamin, M. M., & Lawler, D. F. (2013). *Water Quality Engineering - Physical/Chemical Treatment Processes*. New Jersey: John Wiley & Sons, Inc.
- Bhushan, B. (2009). Biomimetics: lessons from nature - an overview. *Philosophical Transactions of the Royal Society A*, 367, 1445-1486.
- Bunea, F., & Ciocan, G. D. (2018). *Desalination and Water Treatment*. IntechOpen.
- CLO. (2020, 05 07). *Waterwinning en watergebruik in Nederland 1976-2018*. Retrieved from Compendium voor de Leefomgeving: <https://www.clo.nl/indicatoren/nl0057-waterwinning-en-verbruik-nederland>
- Coats, C. (1997, 04). *Viktor Schauberger; The Magic & Majesty of Water*. Retrieved from alivewater.com: <https://www.alivewater.com/viktor-schauberger>
- Danckwerts, P. V. (1953). Continuous Flow Systems. Distribution of Residence Times. *Chem. Engn# Sci. (2)*, 3857-3866.
- Drinkwater Platform. (2020, 08 20). *Waterverbruik in Nederland*. Retrieved from Drinkwaterplatform.nl: <https://www.drinkwaterplatform.nl/waterverbruik-in-nederland-wat-zeggen-de-cijfers/>
- Environmental Dynamics International. (2017). *Technical Bulletin 127 – Energy Consumption and Typical Performance of Various Types of Aeration Systems*. Columbia: Environmental Dynamics International.
- European Standards. (2004, 04). *DIN EN 12255-15 Wastewater treatment plants - Part 15: Measurement of the oxygen transfer in clean water in aeration tanks of activated sludge plants*. Retrieved from European Standards: <https://www.en-standard.eu/din-en-12255-15-wastewater-treatment-plants-part-15-measurement-of-the-oxygen-transfer-in-clean-water-in-aeration-tanks-of-activated-sludge-plants/>
- Gray, N. F. (2010). *Water Technology An Introduction for Environmental Scientists and Engineers*. Oxford: Elsevier Ltd.
- HACH. (2013, 04). *Kuvettentest voor ijzer (II / III), 0,2 - 6,0 mg/l Fe*. Retrieved from HACH: <https://nl.hach.com/kuvettentest-voor-ijzer-ii-iii-0-2-6-0-mg-l-fe/product-downloads?id=26370289274>
- Hill, P. (2017, 01 16). *Lagoon Aeration 101: A video comparison of aeration technologies of aeration technologies*. Retrieved from Triplepoint Water Technologies: <http://www.triplepointwater.com/lagoon-aeration-101/>

- Hoeben, W. F. (2021, 05 05). Personal communication; Interpretation data tracer experiments.
- Innovencio. (2017, 10 02). *Technology Readiness Level (TRL)*. Retrieved from Innovencio: <https://innovencio.nl/technology-readiness-levels/>
- Krupinska, I. (2017). Effect of organic substances on the efficiency of Fe(II) to Fe(III) oxidation and removal of iron compounds from groundwater in sedimentation process. *CIVIL AND ENVIRONMENTAL ENGINEERING REPORTS*; 26 (3), 15-29.
- Levelspiel, O. (2012). *Tracer Technology, Modeling the Flow of Fluids*. New York: Springer.
- Liu, C., Li, S., & Zhang, F. (2011). The oxygen transfer efficiency and economic cost analysis of aeration system in municipal wastewater treatment plant. *Energy Procedia* 5, 2437-2443.
- Manahan, S. E. (2010). *Environmental Chemistry*. Boca Raton: CRC Press Taylor & Francis Group.
- Marjani, A., Nazari, A., & Seyyed, M. (2009). Alteration of Iron Level in Drinking Water by Aeration in Gonbad Kavoods (North East of Iran) . *American Journal of Biochemistry and Biotechnology* 5 (2), 94-97.
- Mulligan, S. (2015). *Experimental and Numerical Analysis of Three-Dimensional Free-Surface Turbulent Vortex Flows with Strong Circulation*. Ireland: Institute of Technology Sligo.
- Mulligan, S., De Cesare, G., Casserly, J., & Sherlock, R. (2018). Understanding turbulent freesurface vortex flows using a TaylorCouette flow analogy. *Scientific reports*, 8(1), 1-14.
- NGWA. (1999). *Unconfined or Water Table Aquifers*. Retrieved from NGWA The Groundwater Association: <https://www.ngwa.org/what-is-groundwater/About-groundwater/unconfined-or-water-table-aquifers>
- NHL Stenden. (2020). *Watertechnologie*. Retrieved from NHL Stenden: <https://www.nhlstenden.com/onderzoek/watertechnologie>
- Pankow, J. F. (1991). *Aquatic Chemistry Concepts*. Chelsea, Michigan: Lewis Publishers, Inc.
- Paul, J. M., Vijayan, A. M., Raju, A., Megha, C. S., & Sadique, K. (2016). Comparison of Iron Removal Efficiency by Aeration and Adsorption. *IOSR Journal of Mechanical and Civil Engineering (IOSR-JMCE;)* Volume 13, Issue 3, 1-4.
- Radlberger, C. (2014). *Der hyperbolische Kegel*. Austria: PKS Eigenverlag.
- Reece, J. B., Urry, L. A., Cain, M. L., Wasserman, S. A., Minorsky, P. V., & Jackson, R. B. (2011). *Cambell Biology: Global Edition*. San Francisco: Pearson.
- Rijksoverheid. (2010, 10 10). *Besluit kwaliteit drinkwater BES*. Retrieved from Wettenbank: <https://wetten.overheid.nl/BWBR0028642/2010-10-10>
- Rosso, D., Stenstrom, M. K., & Larson, L. E. (2008). Aeration of large-scale municipal wastewater treatment plants: state of the art. *Water Sci Technol.*;57(7), 973-8.
- Sharma, S. K. (2001). *Adsorptive Iron Removal from Groundwater*. Lisse: Swets & Zeitlinger B.V.
- Siabi, W. K. (2008). *Aeration and its application in groundwater purification*. WEDC, Loughborough University.

- Şişcanu, N. (2020). *Characterization of a vortex O2 aeration set-up (intern report)*. Leeuwarden: Wetsus.
- Song, Y. (2019). *Characterization of a vortex impeller for aeration (internship report)*. Leeuwarden: Wetsus.
- Stichting Natuur- en Implosietechnieken. (2015). *Walter Schaubberger*. Retrieved 11 01, 2020, from Stichting Natuur- en Implosietechnieken: http://implosie.nl/Walter_Schaubberger.html
- Thacker, N. P., Katkar, S. L., & Rudra, A. (2002). Evaluation of mass-transfer coefficient of free fall cascade-aerator. *Environmental Monitoring and Assessment* 74, 1-9.
- Thakre, S. B., Bhuyar, L. B., & Deshmukh, S. J. (2008). Effect of Different Configurations of Mechanical Aerators on Oxygen Transfer and Aeration Efficiency with respect to Power Consumption. *International Scholarly and Scientific Research & Innovation* 2(2), 170-178.
- Tsuji, K., & Müller, S. C. (2019). *Spirals and Vortices: in Culture, Nature and Science*. Switzerland: Springer Nature.
- TU Delft. (2016, 03 05). *Aeration and gas stripping*. Retrieved from Water treatment: <https://ocw.tudelft.nl/wp-content/uploads/Aeration-and-gas-stripping-1.pdf>
- U.S. Environmental Protection Agency. (2013). *Fiel Measurement of Oxidation-Reduction Potential (ORP)*. Athens, Georgia: U.S. Environmental Protection Agency.
- Unie van Waterschappen. (2018, 01 08). *Waterschappen verkleinen klimaatvoetafdruk*. Retrieved from Unie van Waterschappen: <https://www.uvw.nl/waterschappen-verkleinen-klimaatvoetafdruk/>
- van Beek, C. G., Dusseldorp, J., Joris, K., Huysman, K., Leijssen, H., Schoonenberg Kegel, F., . . . Hofs, B. (2016). Contributions of homogeneous, heterogeneous and biological iron(II) oxidation in aeration and rapid sand filtration (RSF) in field sites. *Journal of Water Supply: Research and Technology - AQUA*; 65 (3), 195-207.
- Van de Griend MSc., M. V., Fuchs, d. C., Wexler, d. D., Loiskandl, p., Woisetschläger, p., & Pečnik, d. (2019, 12). *Vortex treatment of water in a hyperbolic geometry (under review)*. Retrieved from Wetsus: https://www.wetsus.nl/app/uploads/2019/12/appl-w-phys_MvdGriend.pdf
- Vincent, J. F., Bogatyreva, O. A., Bogatyrev, N. R., Bowyer, A., & Pahl, A.-K. (2006). Biomimetics: its practice and theory. *J. R. Soc. Interface* (3), 471-482.
- Vitens. (2021, 03). *Waterkwaliteitsoverzicht: Spannenburg*. Retrieved from Vitens: file:///C:/Users/Esther/Downloads/WZ_NPb%20Spannenburg.PDF
- Warrener, F. (2020). *Vortex impeller based aeration for iron oxidation in groundwater (internship report)*. Leeuwarden: Wetsus.
- Wetsus. (2020a). *About Wetsus*. Retrieved from Wetsus: <https://www.wetsus.nl/about-wetsus/>
- Wetsus. (2020b). *Research Themes: Applied water physics*. Retrieved from Wetsus: <https://www.wetsus.nl/research-themes/applied-water-physics/>
- Whitman, W. G. (1923). The Two-Film Theory of Gas Absorption. *Chemical and Metallurgical Engineering*, 146-148.

Appendix

Appendix I: Composition groundwater and tap water

Table 10 Composition of groundwater and tap water used as feed during the experiments

Test	Groundwater	Tap water (Vitens, 2021)	Units
Chloride	>800	37	mg/L
Inorganic Carbon (IC)	114	55	mg/L
Total Carbon (TC)	135	60	mg/L
Total Organic Carbon (TOC)	20.4	5	mg/L
Iron	4580	<10	µg/L
Manganese	405	<5	µg/L
Sodium (IC)	>400	76.5	mg/L
pH	6.9	7.8	-
Dissolved Oxygen	0.002	9.6	mg/L
Oxidation Reduction Potential	-200	95	mV
Temperature	13	17	°C

Appendix II: Information Experimental setups F01 and F02

Table 11 Dimensions hyperbolic funnels used for experimental setups F01 and F02

Funnel part	Small glass funnel (F01)	Large fibre glass funnel (F02)
Inlet ϕ	17 mm	30 mm
Outlet ϕ	17 mm	30 mm
Cylinder ϕ	300 mm	600 mm
Cylinder height	117 mm	220 mm
Funnel height	940 mm	1290 mm
Total height	1057 mm	1510 mm

Table 12 Sensor information for experimental setups F01 and F02

Sensors	Model	Measuring principle
ORP	Endress+Hauser® memosens orbisint CPS12D	Glass electrode
pH	Endress+Hauser® memosens orbisint CPS11D	Glass electrode
DO	PreSens® PSt3 Sensor	Optical fibre sensor
Flow rate	Endress+Hauser® Picomag DMA25	Electromagnetic
Pressure	Endress+Hauser® Cerabar T PMC131	Ceramic

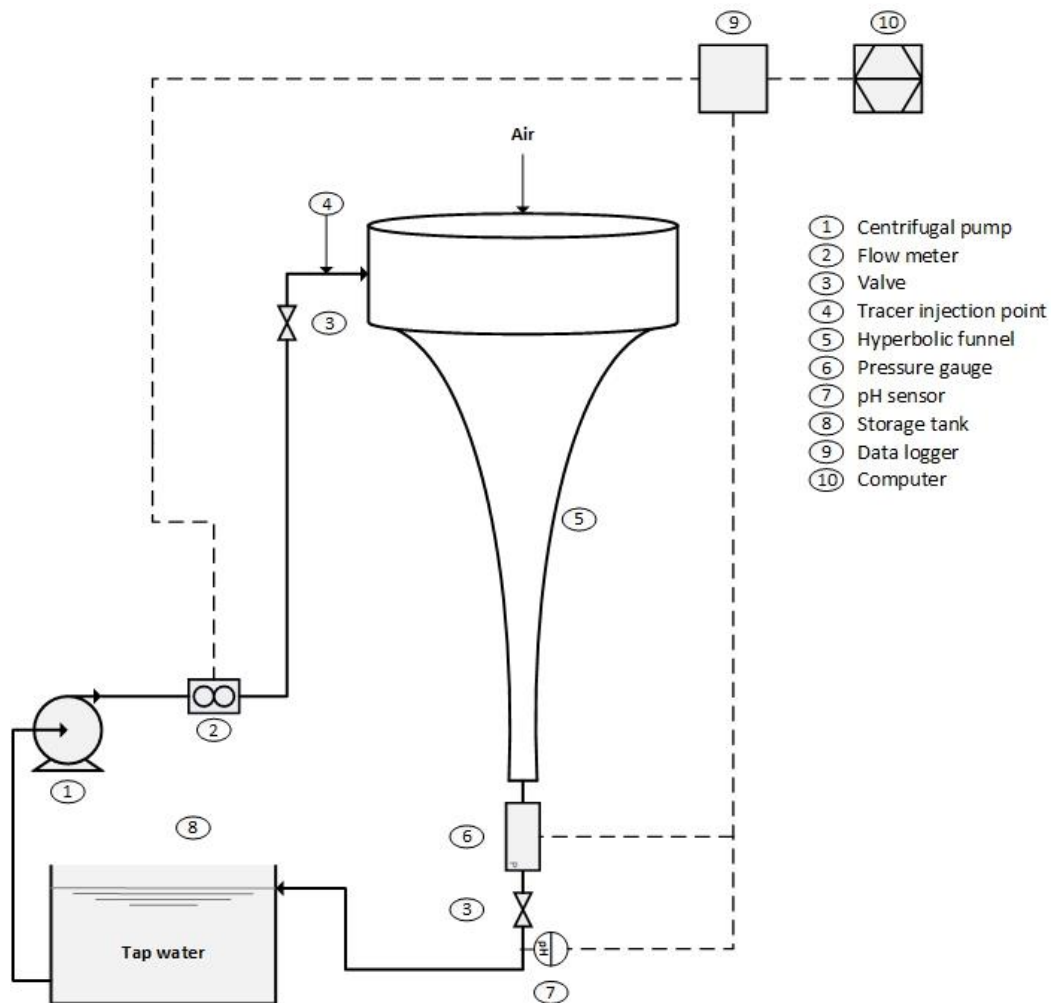


Figure 19 Schematic of setup F02

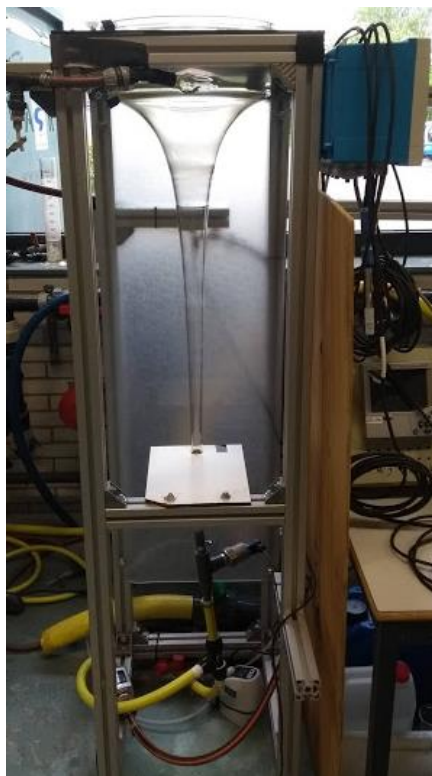


Figure 20 Photographs of Experimental setups; Top) Overview of complete setup, bottom left) setup F01 with glass funnel, bottom right) Setup F02 with large funnel and recirculation

Appendix III: Vortex characteristics and photographs

Table 13 Vortex characteristics for each flow regime and various flow rates

Flow regime		Flow rate (L/min)	Pressure (millibar)	Waterlevel (cm)*	Vortex length (cm)**	Vortex radius (cm)***
RS	RS1	14.7	± 69	3	± 40	15
	RS2	15.2		7	± 50	15
	RS3	15.7		9	± 50	15
TS	TS1	19.9	± 1	2	94	15
	TS2	20.4		5	94	15
	TS3	20.9		7	94	15
SS	SS1	22.0	± 6	11	94	15
	SS2	22.5		11.7	94	10
	SS3	23.0		11.7	94	8

* measured from bottom of cylinder part up

** measured from top hyperbolic part down

*** measured at top of vortex

Table 14 Photographs of the three selected flow rates within the Restricted Schauburger flow regime

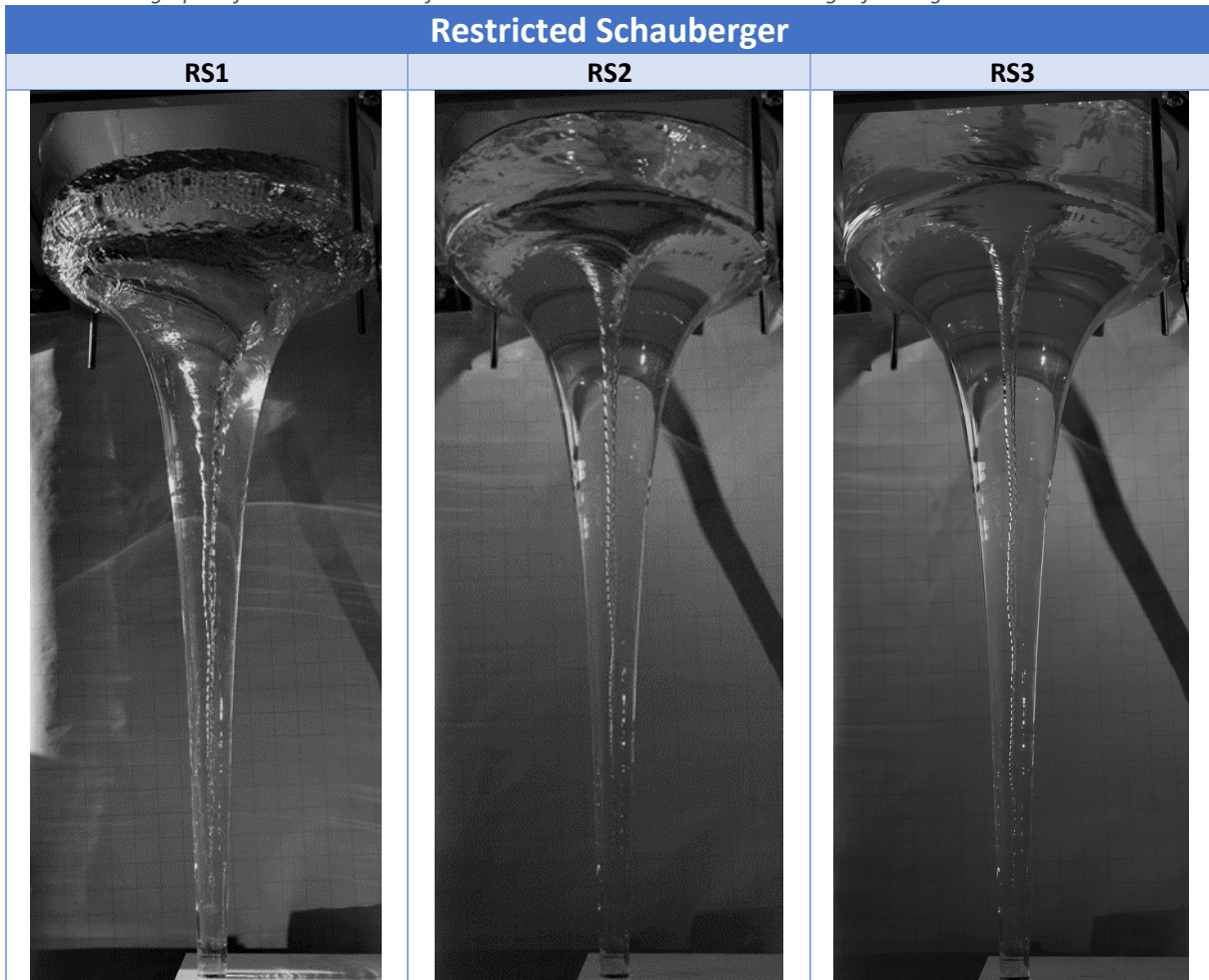


Table 15 Photographs of the three selected flow rates within the Twisted Schauberger flow regime

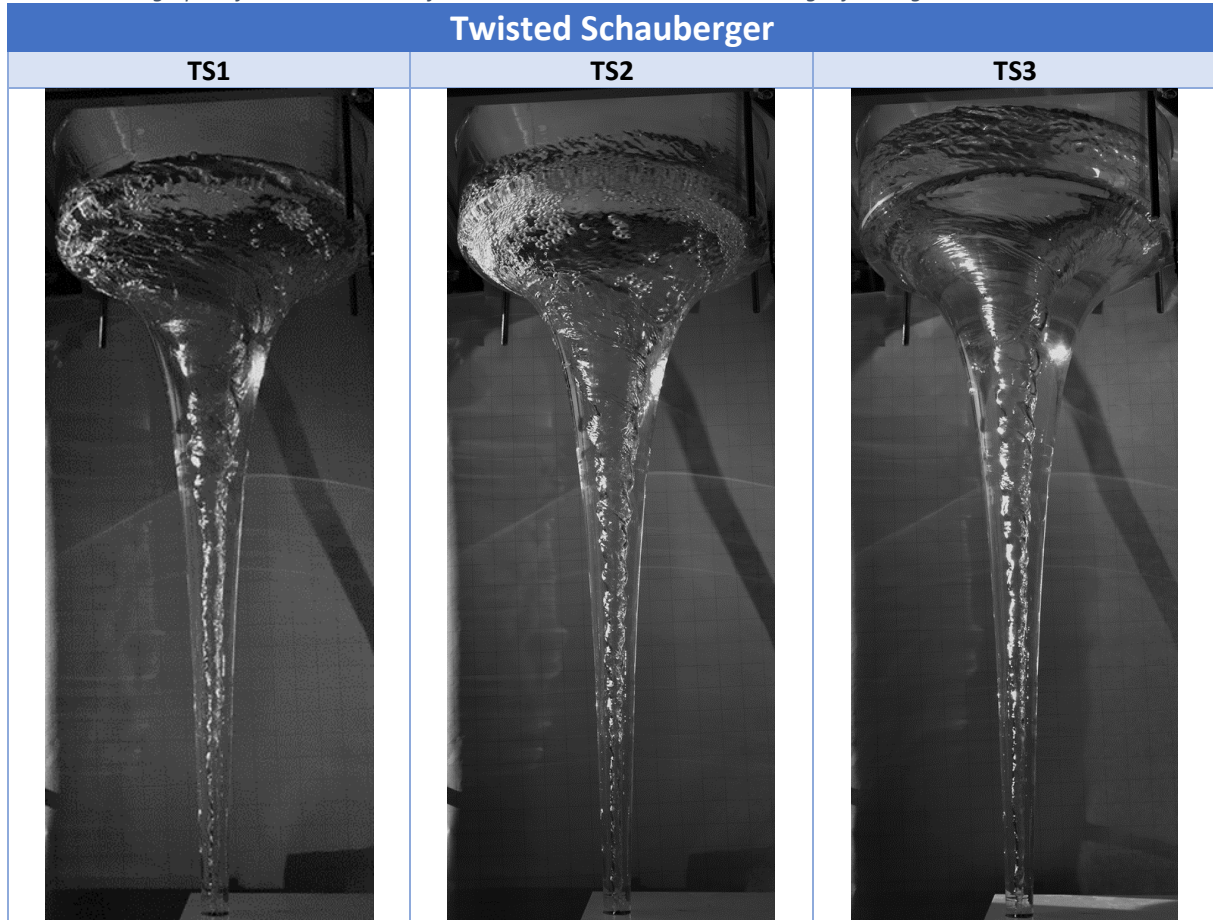
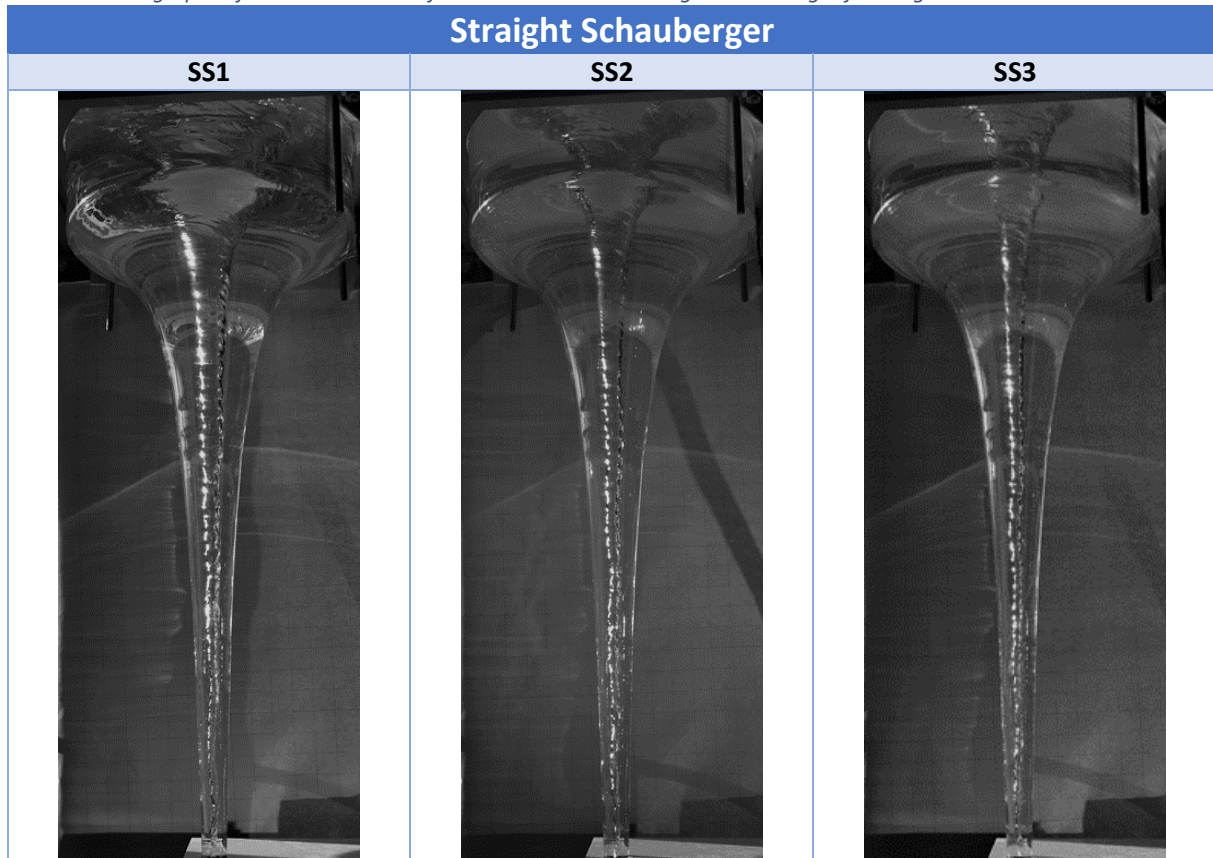


Table 16 Photographs of the three selected flow rates within the Straight Schauberger flow regime



Appendix IV: Data generalization experiments

Table 17 Data for the generalization of each flow regime with various flow rates

Flow regime	Flow rate (L/min)	Pressure (millibar)	V _L (L)	V _{Ratio}	DO outlet (mg O ₂ /L)	ORP outlet (mV)	HRT (sec)
RS	RS1	69.3	5.1	44%	0.86	-145	21
	RS2	68.2	8.2	70%	0.53	-155	33
	RS3	69.6	9.7	82%	0.46	-157	37
TS	TS1	-1.07	4.5	39%	1.84	-126	14
	TS2	1.18	6.3	54%	1.59	-128	19
	TS3	2.46	7.7	65%	1.30	-132	22
SS	SS1	5.18	10.7	91%	1.24	-131	29
	SS2	6.07	11.0	94%	1.22	-130	30
	SS3	6.84	11.1	95%	1.17	-130	29

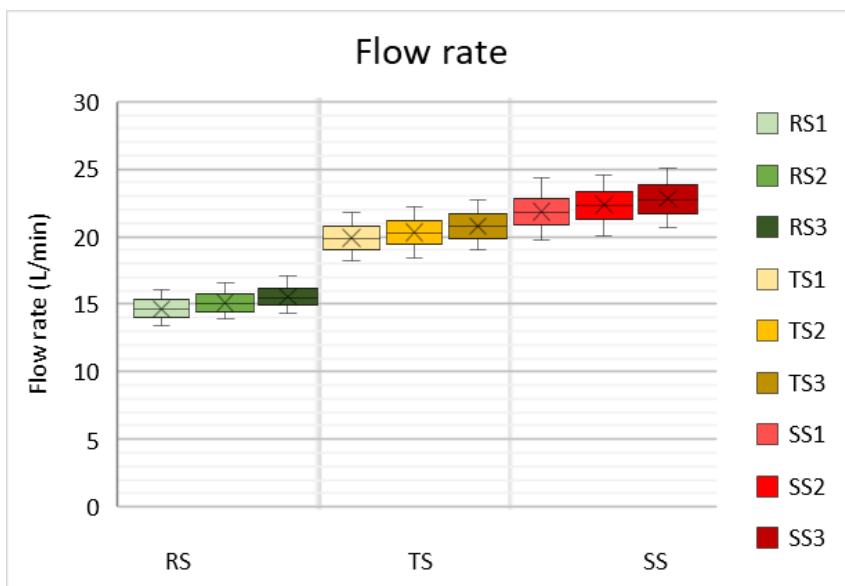


Figure 21 Flow rate measurements per flow regime (F01)

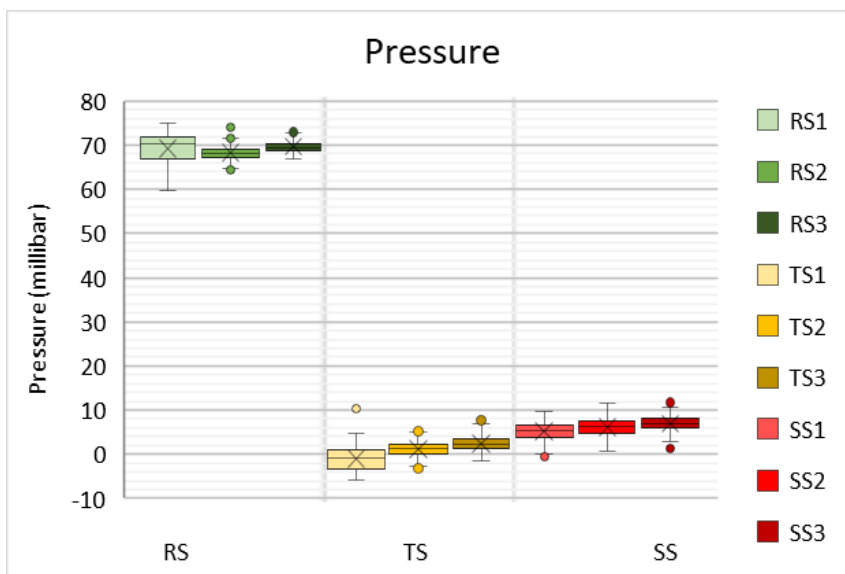


Figure 22 Pressure measurements at the outlet per flow regime (F01)

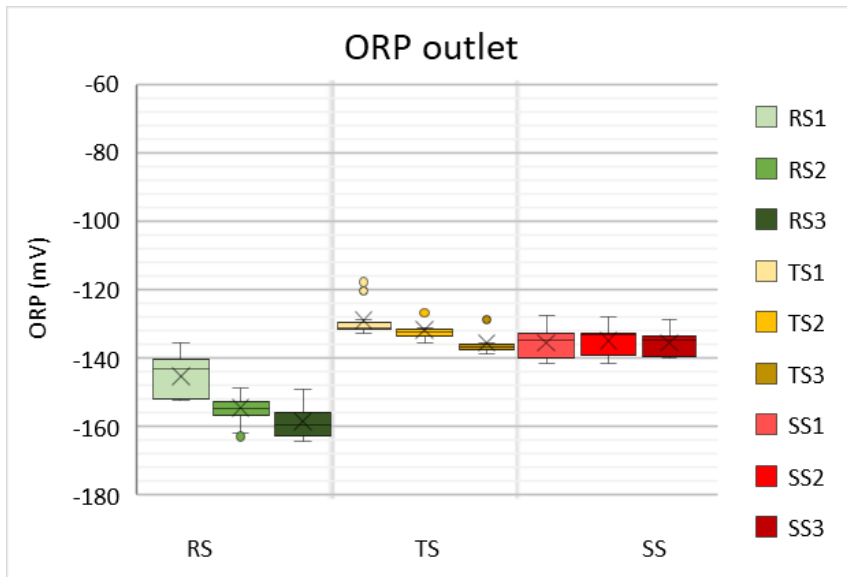


Figure 24 Oxidation Reduction Potential at the outlet per flow regime (F01)

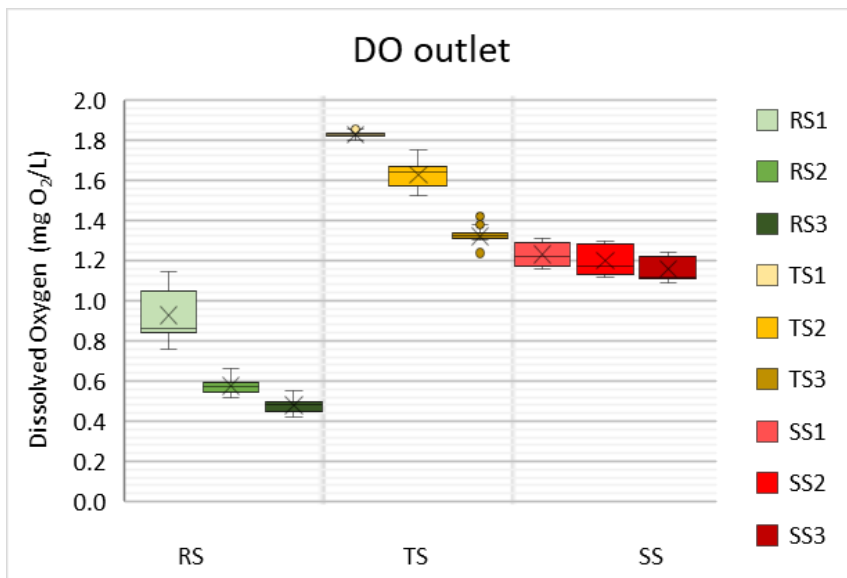


Figure 23 Dissolved Oxygen concentration at the outlet per flow regime (F01)

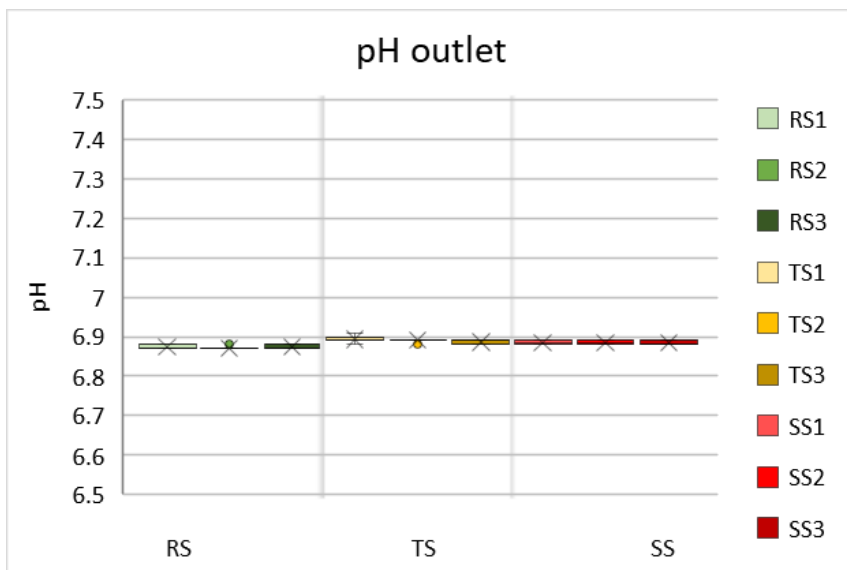


Figure 25 pH at the outlet per flow regime (F01)

Appendix V: Volume calculations hyperbolic funnel and vortices

Calculation total volume hyperbolic funnel (V_T)

Volume of the cylindrical part:

$$V_{cylinder} = \pi \cdot r^2 \cdot h \quad \text{Equation 17}$$

Where r is the radius of the cylinder and h is the height of the cylinder. This gives $V_{cylinder} = \pi \cdot 15^2 \cdot 11.7 = 8.27 \cdot 10^3 \text{ cm}^3 = 8.27 \text{ L}$.

Volume of hyperbolic part:

$$V_{hyperbolic} = \pi \cdot f(x)^2 \cdot dx \quad \text{Equation 18}$$

Where the hyperbolic function $f(x) = \frac{C}{x}$, with $C = 0.008 \text{ m}^2$ as a constant. Placing the hyperbolic funnel upside-down in a graphical plane (with the top facing towards the x-axis) gives the possibility to calculate the volume based on the position of the top and bottom of the funnel (h_1 and h_2) on the y-axis, with the relation $h_1 = \frac{C}{x_1}$ and $h_2 = \frac{C}{x_2}$ and x_1 and x_2 being the radii of the top (0.15 m) and bottom (0.0085 m) of the funnel (see FIGURE 26). Integration of the volume equation gives;

$$V = \int_{h_1}^{h_2} \pi \left(\frac{C}{x}\right)^2 dx = \pi C^2 \int_{h_1}^{h_2} \frac{1}{x^2} \cdot dx = \pi C^2 \left(\frac{1}{h_1} - \frac{1}{h_2}\right)$$

Equation 19

$$V = \pi \cdot 0.008^2 \cdot \left(\frac{1}{0.0533} - \frac{1}{0.941}\right) = 3.56 \text{ L}$$

Equation 20

Because C is based on the outer glass surface of the funnel design, the volume of the glass has to be subtracted from this $V = 3.56 \text{ L}$ to acquire a more accurate result, where the thickness of the glass is assumed to be 1mm;

$$A = 2\pi \int_{h_1}^{h_2} f(x) \sqrt{1 + [f'(z)]^2} dz$$

Equation 21

$$V_{glass} = 1\text{mm} \cdot A = 1\text{mm} \cdot 2\pi C \int_{h_1}^{h_2} \sqrt{\frac{1}{z^2} - \frac{C^2}{z^4}} dz = 1\text{mm} \cdot 2\pi C \int_{h_1}^{h_2} \frac{\sqrt{1 - C^2/z^2}}{z} dz =$$

$$1\text{mm} \cdot 2\pi C \left[\sqrt{h_1^2 - C^2} \left(\frac{\sin^{-1}(h_1/C)}{C\sqrt{1 - h_1^2/C^2}} + \frac{1}{h_1} \right) - \sqrt{h_2^2 - C^2} \left(\frac{\sin^{-1}(h_2/C)}{C\sqrt{1 - h_2^2/C^2}} + \frac{1}{h_2} \right) \right] = 0.14 \text{ L}$$

Equation 22

Therefore the volume of the hyperbolic part of the funnel $V_{hyperbolic} = 3.56 - 0.14 = 3.42 \text{ L}$ and the total volume of the hyperbolic funnel is;

$$V_T = V_{cylinder} + V_{hyperbolic} = 8.27 + 3.42 = 11.7 \text{ L}$$

Equation 23

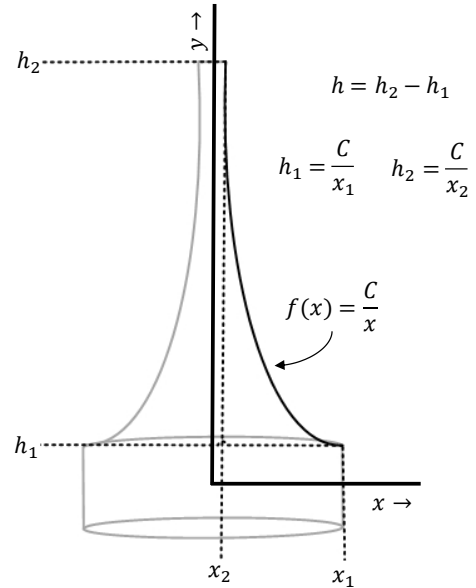


Figure 26 Hyperbolic funnel placed vertically on a graphical plane

Calculation of liquid volume present in the hyperbolic funnel (V_{Liquid} and V_{Filled})

For the first step of calculating V_{Liquid} , the water volume in the funnel is calculated as if there would be no air core present (V_{filled}), thus using the same equations as for calculating V_T . The only difference is the height of the cylinder; this is exchanged for the height of the water level present in the cylindrical part of the funnel. We take the TS2 vortex as an example:

$$V_{cylinder} = \pi \cdot 15^2 \cdot 5 = 3.53 \text{ L} \quad \text{Equation 24}$$

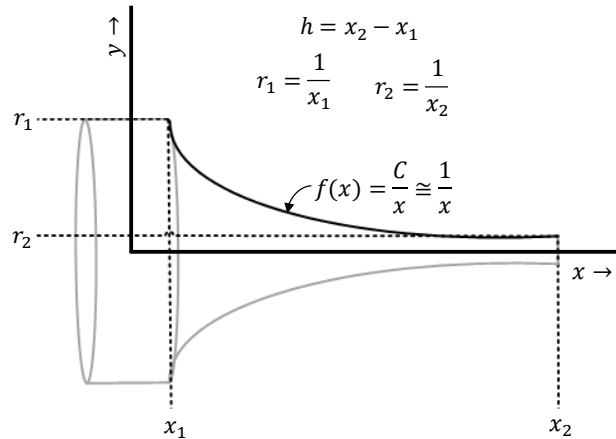


Figure 27 Hyperbolic funnel placed horizontally on a graphical plane

Adding the volume of the hyperbolic part gives:

$$V_{filled} = V_{cylinder} + V_{hyperbolic} = 3.53 + 3.42 = 6.96 \text{ L} \quad \text{Equation 25}$$

Next, the volume of the air core is calculated, assuming that the shape of the vortex follows the hyperbolic function, thus;

$$V_{core} = \pi \cdot f(x)^2 \cdot dx, \quad \text{Equation 26}$$

Where $f(x) = \frac{C}{x} \cong \frac{1}{x}$. However, instead of using the height to calculate the volume, we now use the radii of the top and bottom of the vortex. By placing the vortex horizontally in a graphical plane, with the top orientated towards the y-axis, the vortex volume can be calculated based on the position of the radii of the top and bottom of the vortex (r_1 and r_2) on the y-axis, with the relations $r_1 = \frac{1}{x_1}$, $r_2 = \frac{1}{x_2}$ and $x_2 - x_1 = h$, where x_1 and x_2 are the top and bottom of the vortex and h is the total height of the vortex (see FIGURE 27). Integration of the volume equation gives;

$$V = \int_{x_1}^{x_2} \pi \left(\frac{C}{x}\right)^2 dx = \pi C^2 \int_{x_1}^{x_2} \frac{1}{x^2} \cdot dx = \pi C^2 \left(\frac{1}{x_1} - \frac{1}{x_2}\right) = \pi C^2 \left(\frac{x_2 - x_1}{x_1 \cdot x_2}\right) = \pi C^2 \left(\frac{h}{1/r_1 \cdot r_2}\right) =$$

$$V_{core} = \pi \cdot C^2 \cdot h \cdot r_1 \cdot r_2 \quad \text{Equation 27}$$

When we continue with TS2 as an example, $V_{air} = \pi \cdot 1^2 \cdot (94 + 5) \cdot 15 \cdot 0.15 = 0,70 \text{ L}$. Subtracting V_{core} from the previously calculated water volume V_{filled} gives the liquid volume present in the funnel, in this example when a TS2 vortex is established;

$$V_{Liquid} = V_{filled} - V_{core} = 6.96 - 0.70 = 6.26 \text{ L} \quad \text{Equation 28}$$

The portion of the funnel that is occupied by liquid is determined by dividing V_{Liquid} by V_T . In our example of TS2 this gives;

$$V_{ratio} = \frac{V_{Liquid}}{V_T} = \frac{6.27}{11.7} = 54\% \quad \text{Equation 29}$$

Calculation of Hydraulic Retention Time (HRT)

The calculated liquid volumes were used to estimate the HRT for each flow rate, by using the equation;

$$HRT = \tau = \frac{V}{Q}$$

Equation 30

Where τ is the HRT in minutes, V is the liquid volume in litres and Q of the flow rate in L/min. Using TS2 as an example again, we get a HRT of; $\frac{6.26 L}{20.4 L/min} = 0.307 \text{ min.} = 19 \text{ seconds.}$

Appendix VI: Graphs and calculations tracer experiments

Conversion from pH to Concentration

The constant pH at the start of each pulse experiment was subtracted from each data point to acquire only the increase in pH during each pulse. To graphs de peaks from the pulse experiments in terms of concentration, the datapoints from pH outlet were converted to concentration C_{NaOH} in mg/L. First step is converting from pH to pOH, with;

$$pOH = 14 - pH \quad \text{Equation 31}$$

Based on the pOH, the OH concentration in mol/L was then calculated by;

$$C_{OH} = 10^{-pOH} \quad \text{Equation 32}$$

The concentration in mol/L of NaOH is similar to the concentration of OH based on stoichiometry, thus; $1 \text{ mol/L OH} = 1 \text{ mol/L NaOH}$. Multiplying the concentration of NaOH in mol/L by the molecular weight of NaOH (39997 mg/mol) resulted in a concentration of NaOH in mg/L.

RTD-curves per flow regime

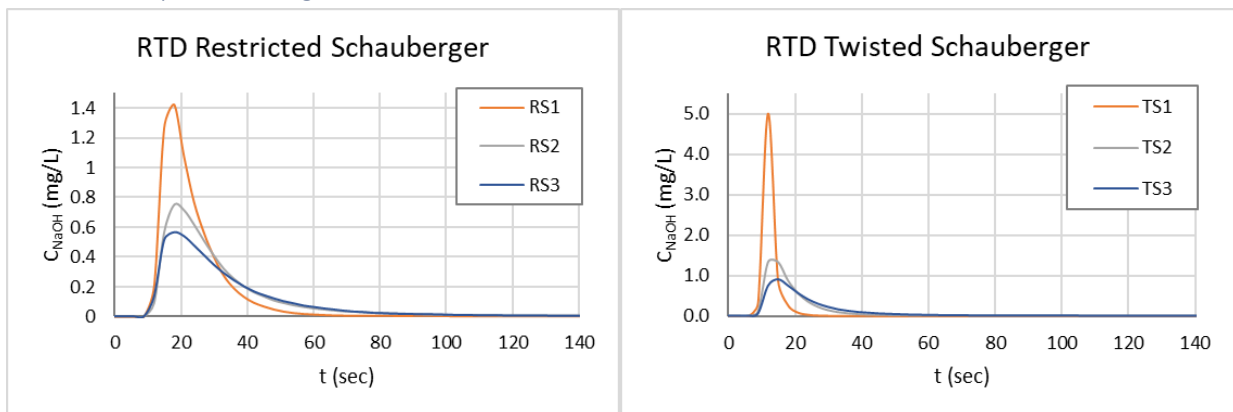


Figure 29 RTD curve of the three flow rates within the RS

Figure 28 RTD curve of the three flow rates within the TS

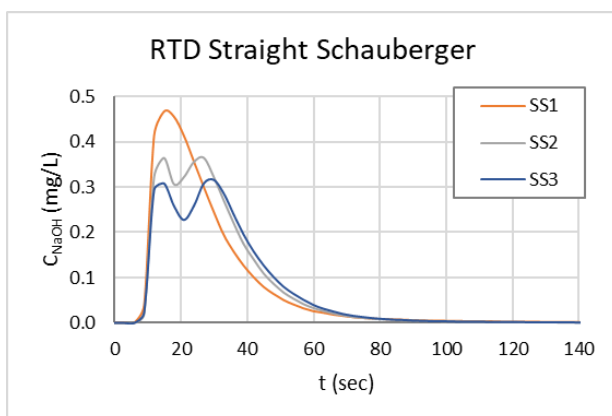


Figure 30 RTD curve of the three flow rates within the SS

Calculations mean residence time and liquid volume (tracer)

Mean residence time (or HRT) was calculated for each pulse using equation;

$$\bar{t} = \frac{\sum t_i C_i}{\sum C_i}$$

Equation 33

Where \bar{t} is the mean residence time in seconds, t_i is the time in seconds and C_i is the concentration of NaOH in mg/L. Next, the liquid volume present in the system during each pulse was determined using equation;

$$V_{L-tracer} = Q \cdot \bar{t}$$

Equation 34

Where $V_{L-tracer}$ is the liquid volume present in the hyperbolic funnel in L, Q is the flow rate in L/min and \bar{t} is the mean residence time in minutes.

Conversion RTD-curves to E_θ -curves

To convert the RTD-curves to E_θ -curves, both the x- and y-axis are made dimensionless. For the y-axis this is done by;

$$E_\theta = \bar{t} \cdot \frac{C_{NaOH}}{A}$$

Equation 35

Where A is the area under the RTD-curve in $\frac{kg/s}{m^3}$, which is determined by;

$$A = \int_0^\infty C \cdot dt \cong \sum_i \bar{C}_i \Delta t_i$$

Equation 36

The x-axis is made dimensionless by;

$$\theta = \frac{t}{\bar{t}}$$

Equation 37

E_{θ} -curves per flow regime

Dimensionless response curves per flow regime, for each flow rate. Included at the bottom right is a graph (Levelspiel, 2012) showing several response curves under closed-closed conditions for various dispersion numbers for compaction. The curves for the hyperbolic funnel show similarities with curves of the dispersion numbers 0.1 to 0.02.

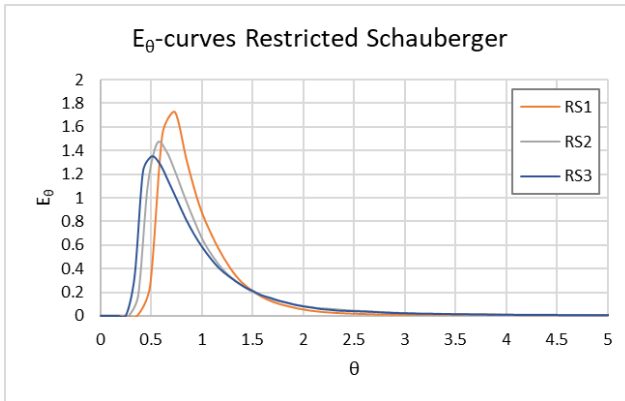


Figure 33 E_{θ} curve of the three flow rates within the RS

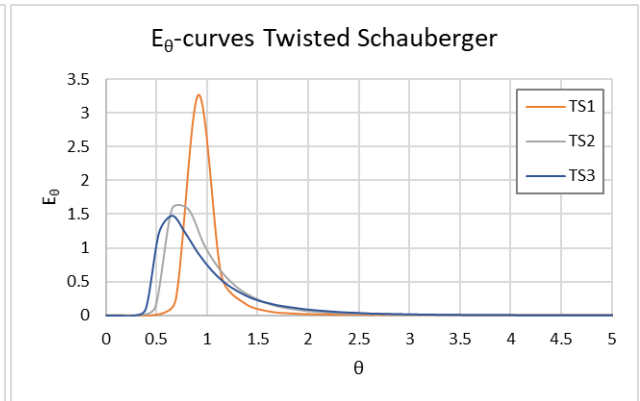


Figure 32 E_{θ} curve of the three flow rates within the TS

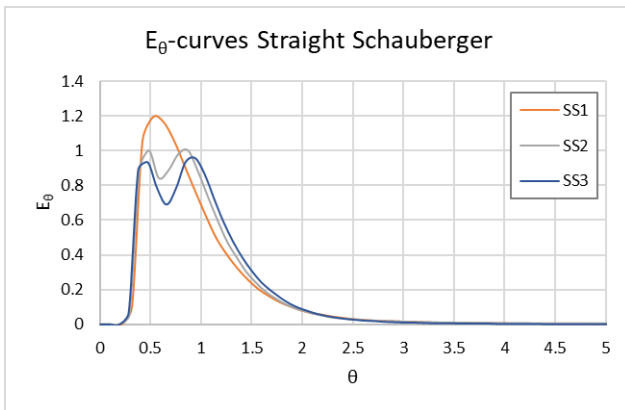


Figure 31 E_{θ} curve of the three flow rates within the SS

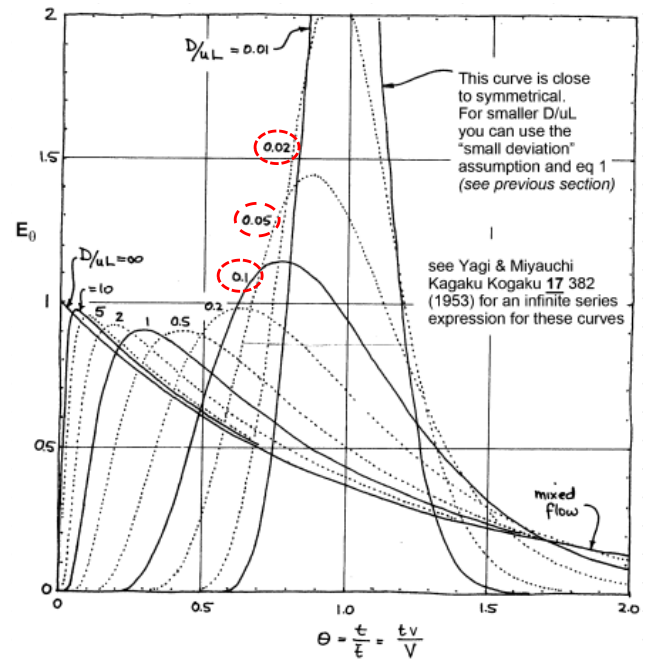


Figure 34 Multiple E_{θ} curves with their corresponding D/uL values (Levelspiel, 2012)

Appendix VII: Results water sample analysis iron oxidation efficiency

Table 18 Iron concentrations inlet and outlet for each flow regime at pH 6.9 (no pH control)

pH	Flow regime	Inlet (mg/L)			Outlet (mg/L)		
		Fe ²⁺	Fe ³⁺	Fe _{Tot}	Fe ²⁺	Fe ³⁺	Fe _{Tot}
6.9	RS	4.55	0.2	4.75	4.32	0.398	4.72
		4.56	0.189	4.75	4.34	0.355	4.69
	TS	4.54	0.246	4.79	4.13	0.564	4.7
		4.56	0.216	4.77	4.14	0.563	4.71
	SS	4.55	0.184	4.74	4.23	0.449	4.68
		4.52	0.185	4.7	4.22	0.479	4.7

Table 19 Iron concentrations inlet and outlet for each flow regime at pH 7.3

pH	Flow regime	Inlet (mg/L)			Outlet (mg/L)		
		Fe ²⁺	Fe ³⁺	Fe _{Tot}	Fe ²⁺	Fe ³⁺	Fe _{Tot}
7.3	RS	4.54	0.234	4.78	4.3	0.385	4.69
		4.54	0.21	4.75	4.25	0.466	4.71
	TS	4.55	0.185	4.74	4.1	0.658	4.76
		4.54	0.21	4.75	3.96	0.776	4.73
	SS	4.54	0.234	4.78	4.17	0.552	4.72
		4.53	0.232	4.76	4.09	0.612	4.7

Table 20 Iron concentrations inlet and outlet for each flow regime at pH 7.7

pH	Flow regime	Inlet (mg/L)			Outlet (mg/L)		
		Fe ²⁺	Fe ³⁺	Fe _{Tot}	Fe ²⁺	Fe ³⁺	Fe _{Tot}
7.7	RS	4.54	0.234	4.78	4.26	0.45	4.7
		4.54	0.21	4.75	4.23	0.479	4.7
	TS	4.55	0.185	4.74	3.94	0.754	4.69
		4.54	0.21	4.75	3.92	0.748	4.66
	SS	4.54	0.234	4.78	4.16	0.567	4.72
		4.53	0.232	4.76	4.06	0.62	4.68

Table 21 Iron concentrations inlet and outlet for each flow regime at pH 8.1

pH	Flow regime	Inlet (mg/L)			Outlet (mg/L)		
		Fe ²⁺	Fe ³⁺	Fe _{Tot}	Fe ²⁺	Fe ³⁺	Fe _{Tot}
8.1	RS	4.58	0.187	4.76	4.25	0.453	4.7
		4.56	0.175	4.74	4.29	0.412	4.7
	TS	4.52	0.249	4.77	3.72	0.944	4.66
		4.51	0.22	4.73	3.67	0.963	4.63
	SS	4.61	0.165	4.78	4.08	0.625	4.7
		4.56	0.185	4.74	4.06	0.615	4.67

Table 22 Iron concentrations inlet and outlet for each flow regime at pH 8.5

pH	Flow regime	Inlet (mg/L)			Outlet (mg/L)		
		Fe ²⁺	Fe ³⁺	Fe _{Tot}	Fe ²⁺	Fe ³⁺	Fe _{Tot}
8.5	RS	4.54	0.234	4.78	3.97	0.725	4.68
		4.54	0.21	4.75	3.9	0.771	4.67
	TS	4.55	0.185	4.74	3.51	1.17	4.68
		4.54	0.21	4.75	3.14	1.51	4.65
	SS	4.54	0.234	4.78	3.88	0.844	4.72
		4.53	0.232	4.76	3.7	0.937	4.63

Table 23 Iron concentrations inlet and outlet for each flow regime at pH 8.9

pH	Flow regime	Inlet (mg/L)			Outlet (mg/L)		
		Fe ²⁺	Fe ³⁺	Fe _{Tot}	Fe ²⁺	Fe ³⁺	Fe _{Tot}
8.9	RS	4.54	0.234	4.78	3.96	1.72	4.68
		4.54	0.21	4.75	2.6	2.05	4.64
	TS	4.55	0.185	4.74	0.768	3.86	4.63
		4.54	0.21	4.75	0.976	3.62	4.59
	SS	4.54	0.234	4.78	2.25	2.39	4.64
		4.53	0.232	4.76	2.26	2.38	4.64

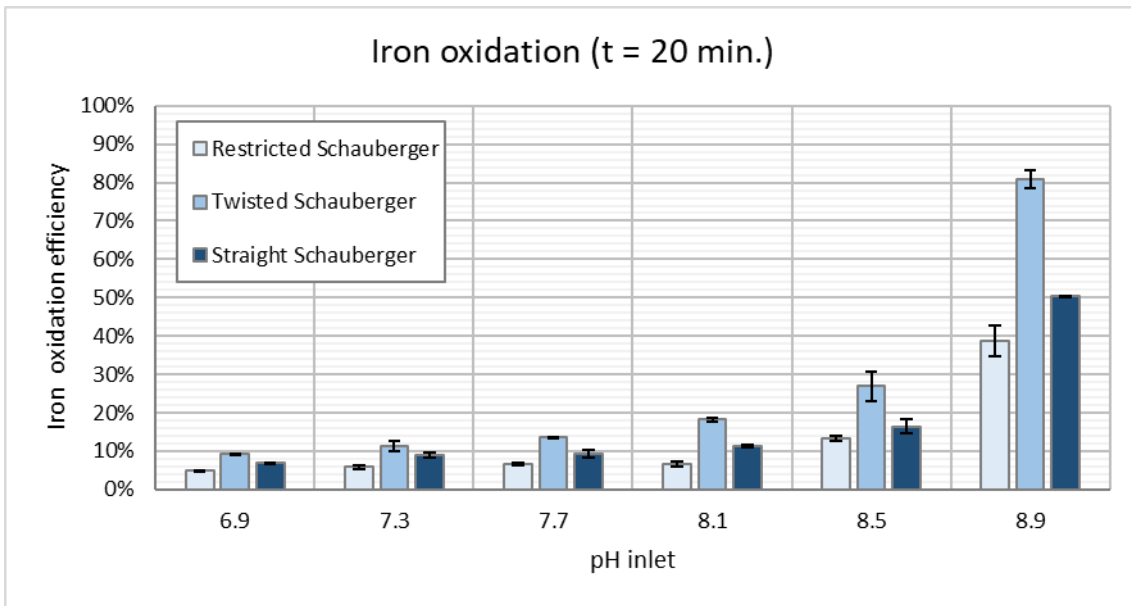


Figure 35 Iron concentration efficiencies for each flow regime and pH condition, after 20 minutes contact time of outlet sample

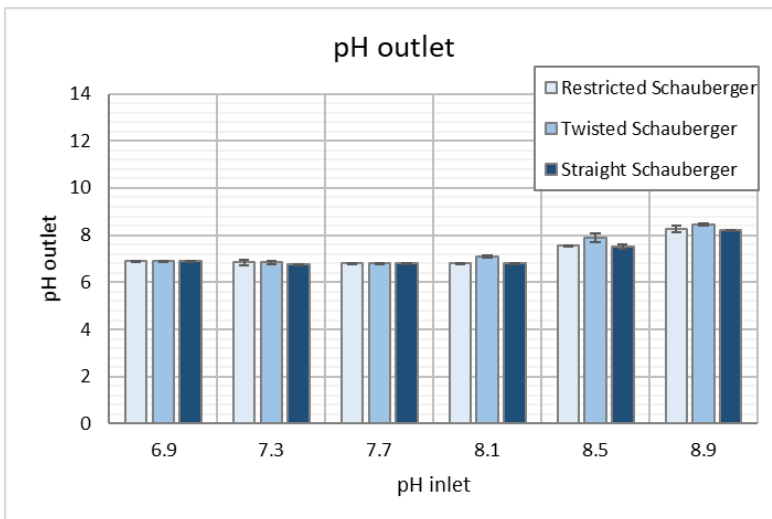


Figure 36 pH at the outlet during the iron oxidation experiments

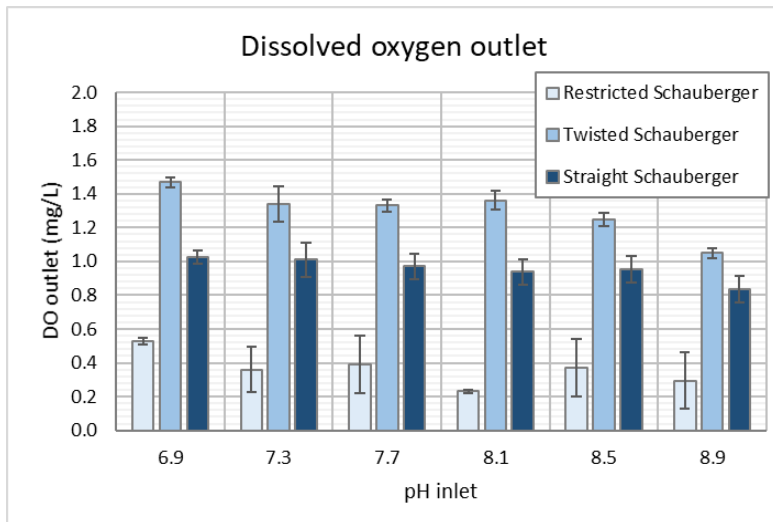


Figure 38 Dissolved oxygen at the outlet during the iron oxidation experiments

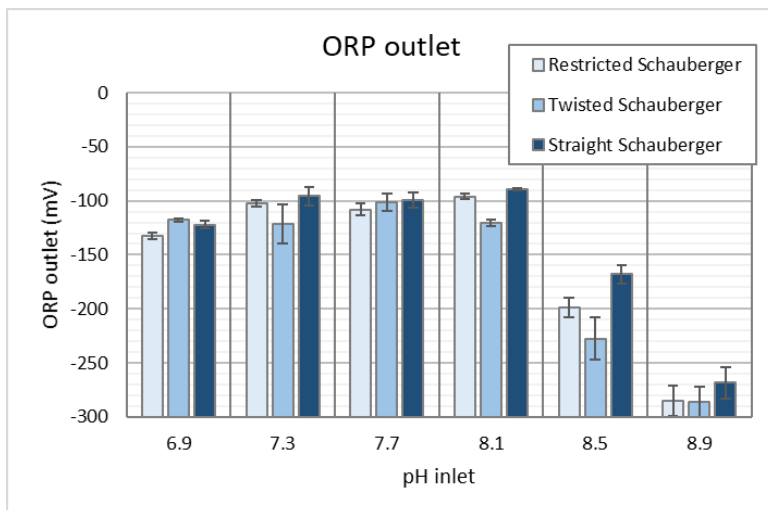


Figure 37 Oxidation Reduction Potential at the outlet during the iron oxidation experiments